Instituto Tecnológico y de Estudios Superiores de Monterrey

Campus Monterrey

School of Engineering and Sciences


# *Opuntia ficus-indica* L. Mill Nanofibers as a Potential Scaffold for Bone Regeneration

A thesis presented by

Kathya Huesca Urióstegui

Submitted to the

School of Engineering and Sciences

in partial fulfillment of the requirements for the degree of

Master of Science

In

Biotechnology

Monterrey Nuevo León, June 14th, 2021

## Dedication

*To my parents, nothing would've been possible without you and I know it hasn't been an easy task. Thanks for your effort and the sacrifices made so I could be right here, and for your trust in me, my dreams and my decisions. Specially, thank you for your unconditional support and love.*

*To Alinne, for always being on the lookout for me and caring about my progress. Thanks for your support from a distance and for being available to listening to me, understanding me and even giving me your advices and calming me down.*

*Love you, all this is for and to you.*

**Acknowledgements**

First of all, I would like to acknowledge Dr. Marilena Antunes and Dr. Daniel Guajardo for letting me participate in this project and contributing to my personal and professional development. Thank you for always being patient and being as immersed as I was in this project, and always being available to solve my doubts and guiding me through this process. I will always appreciate your time, encourgament and advices given during this time.

Also I want to thank Ale, Ana and Antonio for your company through this ride. Thank you for making this hard time lighter and for your encourgament, friendship and support. I'll always cherish our time together and appreaciate the long writing nights that led to long lasting bonds.

Likewise, I want to thank Nestor for the unconditional support through the years. Thanks for sharing this experience with me and for always encouraging me to be my best version and aim high for my dreams; for celebrating even more than me my victories and for always being by my side.

Finally, I would like to acknowledge M.C. Laura E. Gómez Lizárraga and the Instituto del Mar y Limnología (UNAM) for their assistance with the Scanning Electron Microscopy service.

I would like to thank to the Consejo Nacional de Ciencia y Tecnología (CONACYT) for scholarship (CVU 934639) and the Tecnológico de Monterrey for the academic scholarship and to NutriOmics focus group for their economic support.

***Opuntia ficus-indica* L. Mill Nanofibers as a Potential Scaffolds for Bone Regeneration**

by
Kathya Huesca Urióstegui

# Abstract

Bone is the second most commonly transplanted tissue in the world due to bone loss, however, some aggressive effects have shown in the current alternatives for its treatment. Current research has been directed at the development of scaffolds with biocompatible materials, with the ability of assisting in the bone healing process and be resorbed in the body. This work focused on the development of an electrospun nanofiber mesh loaded with isorhamsnetin glycosides (IGs) from *Opuntia ficus-indica* (OFI) flour and its evaluation as scaffold for adhesion and maturation of human osteoblasts hFOB and its impact in bone regeneration *in vitro* by the assessment of mineralization markers. Electrospun nanofibers were developed with the parameters of 15 cm, 20kV, 1mL/h, followed by the addition of 10%, 30%, 50% and 70% w/w of OFI flour. Next, the fibers were characterized chemical and morphologically by FTIR and SEM, and its swelling capacity and degradation rate, as well as its release kinetics were assessed. Finally, biological assays *in vitro* were carried: cell cytotoxicity, calcium deposition and ALP activity. The best nanofiber obtained was PLA loaded with 70% w/w of OFI flour since it presented characteristics such as fiber alignment and smooth surface. It had a content of 904.33 µg IsoEq/g fiber and 14.9% release rate of IGs in 48h, a swelling ratio of 89.99% after 24h and 13.03% of degradation rate in 48h. It didn't show significant cytotoxicity and had evidence of mineralization and calcium deposition, so it can be considered as scaffold for adhesion and maturation of human osteoblasts hFOB and its impact in bone regeneration *in vitro*.

Keywords: *PLA electrospun nanofibers, scaffold, isorhamnetin glycosides, hFOB maturation, bone regeneration.*

## List of Figures

## List of Tables

**Contents**

# Introduction

Every year, an approximate of 4 million surgical procedures involve bone grafts or substitutes, making bone the second most commonly transplanted tissue in the world (Jindal et al., 2020). Bone loss is caused by several reasons such as trauma, tumors, congenital diseases and aging, which is why it is considered a major worldwide health problem (Hokmabad et al., 2019). Some consequences of bone loss are enhanced bone fragility, followed by an increase in fracture risk, which levels off after the age of 60 years, causing morbidity, disability and could lead to premature death. Additionally, it represents a considerable economic burden on health services, costing many billions of dollars each year (Prentice, 2004).

Metal implants such as plates and screws have been used to repair bone fractures since around 1895, mostly from alloys such as Cobalt (Co) and Titanium (Ti)-based (Murr, 2017). These metallic biomaterials (Co, Ti, iron (Fe), among others) have become essential for orthopedic purposes due to their low cost and excellent mechanical properties. However, due to corrosion, some side effects have been shown like the inhibition the immune system, or the induction of the formation of free oxygen radicals, spreading it through the whole body via lymph and blood (Ferreira et al., 2003).

Because of this, current research has been directed at the development of scaffolds with biocompatible and biomimetic materials to replace bone, with the ability of assisting in the healing process and dissolve in the body to be replaced by the patient's own tissue. An ideal scaffold should guide and assist in tissue formation when implanted in the affected site, must be from a three-dimensional material, with pore sizes around 260 μm. In addition, it must promote successful ingrowth of the surrounding tissue, and should assist both in the recruitment process of patient's own cells to be resorbed by osteoclasts overtime, and at the same time, they should assist the osteoblasts while depositing newly mineralized bone (Preez et al., 2018).

In order to promote cell proliferation, and in addition to said qualities, some biological requirements must be monitored. First, there must be production of Nitric Oxide (NO), since it's a signal of possible early increased formation of bone. On the other side, an increase in the intracellular calcium concentration may lead to a

decrease in cell proliferation (Preez et al., 2018). Additionally, an important differentiation factor is the Bone Morphogenetic protein-2 (BMP-2), due to its capacity of inducing bone regeneration and modulating osteoblastic differentiation through different pathways (Huang et al., 2014). These pathways could be affected by TNF-$\alpha$ and IL-1$\beta$, major cytokines that stimulate MAPK activation in inflammatory environment, promoting bone loss and a decrease in mineral density by inhibiting osteoblastic differentiation and bone formation, which are suspected causes of low osteo-inductive efficacy of BMP-2 (Huang et al., 2014).

Owing to this, current research has rapidly shifted from synthetic bone and tissue grafts, to the application of porous biodegradable and bioactive implants or scaffolds which allow the cells to adhere, grow, proliferate and, subsequently, secrete extracellular matrix (ECM) proteins, providing unique advantages like the ability to accommodate cells, allowing mass-transport between implant and surroundings, promoting cell migration, attachment, vascularization, and supporting bone growth from within the scaffold material (Jindal et al., 2020).

An example of a matrix that provides bioactive compounds suitable for this application is *Opuntia ficus-indica* (OFI), which is an important medicinal plant best known for its beneficial health effects, including wound-healing, immunomodulatory, antioxidant, among others (Santos-Zea et al., 2011). Most importantly, OFI has been studied for its anti-inflammatory effects, which have been attributed to its most abundant flavonoids, the isorhamnetin glycosides, since they significantly reduce proinflammatory biomarkers (Antunes-Ricardo, Gutiérrez-Uribe, López-Pacheco, et al., 2015; Antunes-Ricardo, Gutiérrez-Uribe, Martínez-Vitela, et al., 2015). There is also some evidence that OFI is an important source of calcium and may have potential for applications in the prevention and treatment of diseases associated with calcium deficiency (Contreras-Padilla et al., 2011).

These results suggest that the last trends are focused on the incorporation of bioactive extracts to a biocompatible scaffold. Given this, OFI comes out as an excellent source of calcium and potential anti-inflammatory bioactive compounds for its incorporation to novel delivery systems such as nanofibers, for future medical

applications like scaffolds which could aid the proliferation of osteoblasts cells, giving an efficient and more economical solution to the treatment of bone loss.

# Hypothesis

The development of an electrospun nanofiber mesh loaded with isorhamnetin glycosides from *Opuntia ficus-indica* (OFI) flour will promote cell adhesion and maturation on human osteoblast hFOB *in vitro* by the assessment of mineralization markers.

# Objective

Evaluate the effect of an electrospun nanofiber mesh loaded with isorhamnetin glycosides from *Opuntia ficus-indica* flour as scaffold for adhesion and maturation of human osteoblasts hFOB and its impact in bone regeneration *in vitro*.

## Specific Objectives

- Determine the process parameters such as flow rate, biopolymer (Polycaprolactone (PCL), Polylactic acid (PLA), Polymethylmethacrylate (PMMA)), voltage, distance and time of nanofiber elaboration by electrospinning.
- Evaluate the effect of the addition of *Opuntia ficus-indica* (OFI) flour in the electrospun nanofibers with a determined biopolymer (PCL/PLA/PMMA) in their chemical and biological properties.
- Determine isorhamnetin glycosides content and release in the nanofiber loaded with OFI flour by drug release kinetics *in vitro* using High Performance Liquid Chromatography coupled with Diode-Array Detector (HPLC-DAD).
- Characterize the nanofiber mesh morphology by Scanning Electron Microscope (SEM).
- Characterize the nanofiber mesh chemical structure by Fourier-Transform Infrared Spectroscopy (FTIR).
- Determine water capacity percentage of the electrospun nanofiber by the gravimetric swelling test.
- Evaluate biodegradation capacity of electrospun nanofiber by gravimetric weight loss.

- Evaluate cytotoxicity of electrospun loaded nanofiber on human osteoblasts (hFBO) cell line.
- Determine human maturation of human osteoblasts (hFOB) growth on electrospun nanofibers by the measuring of alkaline phosphatase activity (ALP).
- Determine calcium deposition by human osteoblasts (hFOB) growth on electrospun nanofibers by Calcein-AM staining assay.

# 1. Background

# 1. Woven Bone

Woven bone is a tissue produced during skeletal histogenesis and growth, is rapidly formed during fracture healing and in response to high doses of anabolic agents (Hernandez et al., 2004). Bone is a dynamic living tissue loosely organized, consisting of several nanostructures. Mainly it is composed of nanocrystal of hydroxyapatite, dispersed in a matrix of collagen I (Preez et al., 2018). One of the major constituents in bone and other mineralized vertebrate tissues are apatite crystal, which accounts for about 65% weight (wt) of bone and provides most of the stiffness and strength of bone (Su et al., 2003).

This is the only body tissue capable of regeneration, since it is in constant formation and resorption, it allows the renovation of 5-15% of total bone mass per year, under normal conditions. In this remodeling process, new bone, identical to the pre-existing, is formed. Treatment in the event of a fracture or bone graft, in traumatology, orthopedics, implantology and maxillofacial and oral surgery, is based on the biological principles of bone regeneration, which involves cells, extracellular matrix (ECM), and osteoinductive signals (Hernández-Gil et al., 2006)

## 1.1 Bone proliferation

Bone cells are found within bone tissue or in the conjunctive stroma of the bone marrow. There are five different types of cells that can originate from these stem cells: fibroblasts, osteoblasts, chondroblasts, adipocytes and myoblasts, according to the different molecular signals that initiate activation cascade of different genes (Hernández-Gil et al., 2006).

### 1.1.1 Osteoblastic differentiation and cell proliferation

An important differentiation factor is the Bone Morphogenetic protein-2 (BMP-2), which constitute one the most powerful regulators of osteoblastic differentiation from mesenchymal stem cells (Hernández-Gil et al., 2006). It is capable of inducing bone regeneration by promoting endochondral ossification and modulates

osteoblastic differentiation through the BMP/Smad pathway, which is initiated by type II BMP receptors that phosphorylate BMP-specific Smad 1/5/8 and propagate BMP signals. Promptly, this Smad 1/5/8 binds to Smad4 and makes a complex, which is then transported to the nucleus to activate or repress transcription of osteogenic genes (Huang et al., 2014).

Another pathway to modulate osteoblastic differentiation is the BMP pathway through Mitogen-activated protein kinase (MAPK) cascades. In this pathway, BMP-2 activates signaling pathways of a set of MAPKs: extracellular signal-regulated kinase (ERK) 1/2, p38 protein, and Jun-N terminal kinases (JNK) 1/2, which promotes expression and activation of osteogenic-specific transcription factor runt-related transcription factor 2 (Runx2), that has an essential role in osteoblastic differentiation of stem cells, since it directly stimulates transcription of its downstream genes osteocalcin (OCN), type I collagen (COL1A1), and osteopontin (OPN), by binding to specific enhancer regions containing core sequence (Huang et al., 2014). It is first detected in pre-osteoblasts, and its expression increases in immature osteoblasts, in mature osteoblasts there's no significant concentration of Runx2 protein (**Figure 1**) (Komori, 2009).

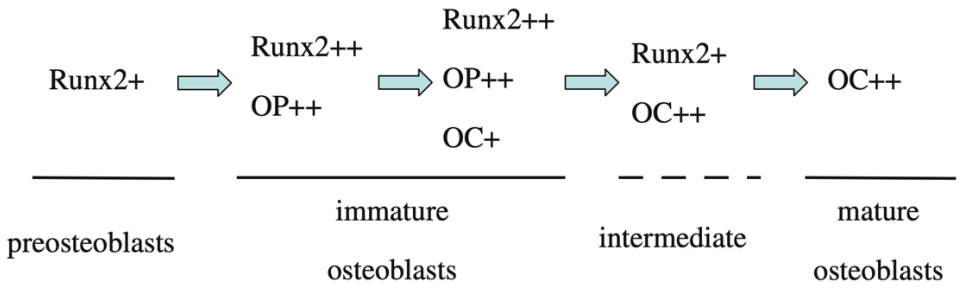


***Figure 1.*** *Runx2 protein expression during osteoblast differentiation. OP: osteopontin, OC: osteocalcin, from (Komori, 2009).*

In early stages, skeletal component cells are derived from mesenchymal stem cells. Different transcription factors determine their lineages (**Figure 2**) (Komori, 2006).

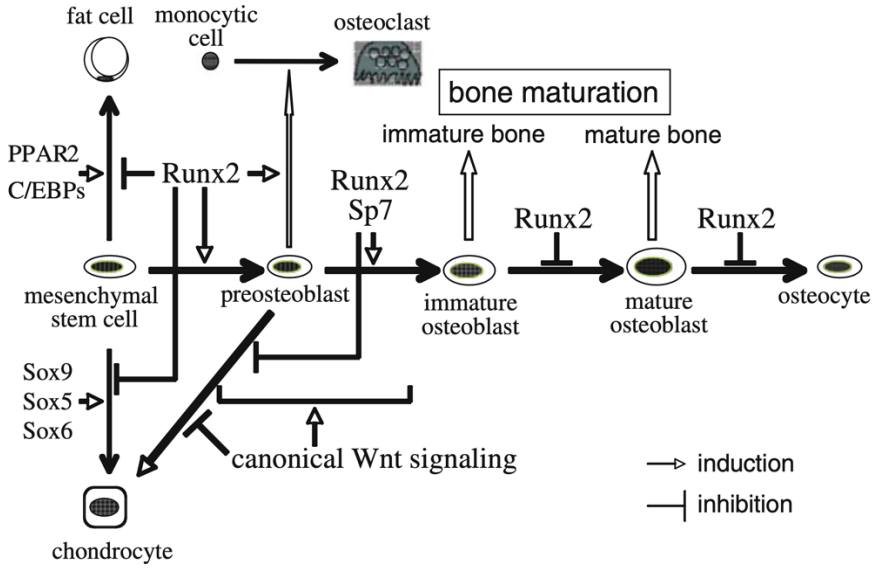


***Figure 2.*** *Regulation of osteoblast differentiation by different transcription factors, from (Komori, 2009).*

In addition, Cbfa1 is the first indicator of osteogenic differentiation, followed by the early expression of Collagen I, OPN, and alkaline phosphatase (ALP), which is a surface protein that permits the mineralization and participates in the regulation of proliferation, migration and differentiation of osteoblastic cells (Hernández-Gil et al., 2006).

On the other hand, the organic matrix, or osteoid material, constitutes one third of the bone mass, and it is mainly formed by proteins, especially collagen (90%) (**Table 1**) (Hernández-Gil et al., 2006). The mineralized ECM is more than just an inert support for bone cells. It serves as an important reservoir for growth factors, and provides a source of markers to monitor the activities and health status of bone tissue (Young, 2003).

***Table 1.*** *Osteoid matrix proteins, from (Hernández-Gil et al., 2006).*

| **Protein** | **Types** |
|---|---|
| Collagen | • Type I, III, V, XII |
| Proteoglycans | • Chondroitin-sulphate<br>• Decorin<br>• Biglycan<br>• Hyaluronan |

| | |
|---|---|
| Proteins with γ-carboxyglutamic acid | • Osteocalcin<br>• Matrix protein with γ-carboxyglutamic acid |
| Glycoproteins | • Osteonectin<br>• Alkaline phosphatase<br>• Proteins with RGD:<br>Fibronectin<br>Thrombospondin<br>Osteopontin<br>Vitronectin<br>Bone sialoprotein |
| Proteins from plasma | • Albumin<br>• α2-SH-glycoprotein |
| Growth factors | • Insulin-like Growth Factor (IGF)-I, II<br>• Transforming Growth Factor (TGF)-β<br>• Platelet Derived Growth Factor (PDGF) |

### 1.1.2 Inflammation and Bone Proliferation

There are three known phases that characterize bone healing: the inflammatory phase, the repair phase, and the remodeling phase, all three which partially overlap (**Figure 3**). Successful healing is highly dependable on the initial inflammatory phase, which is key for robust bone healing (Maruyama et al., 2020).

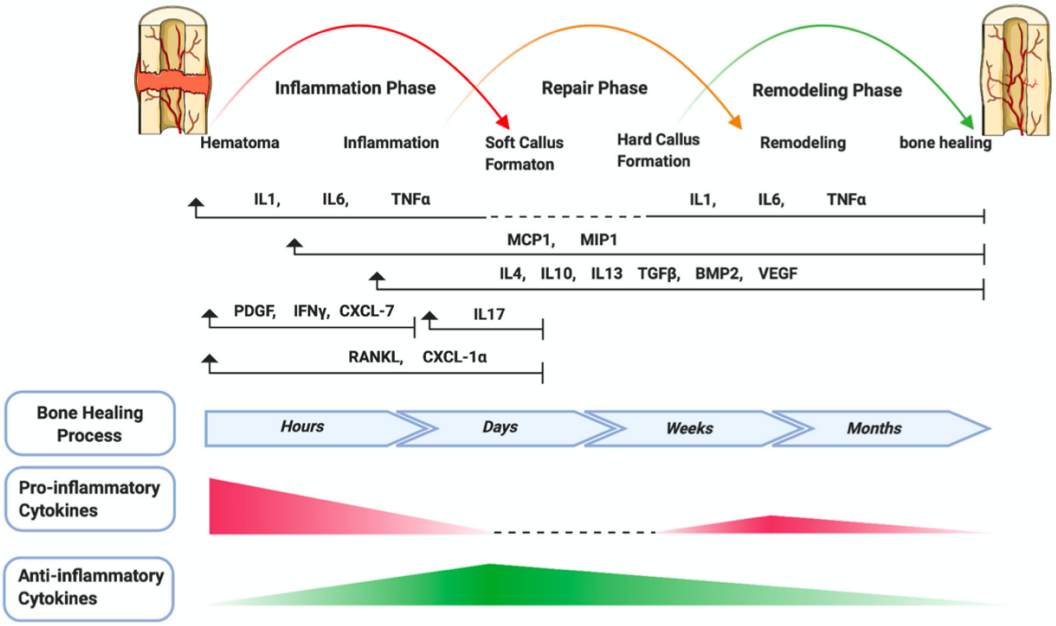


***Figure 3.*** *Schematic summary of the stages of bone healing with temporal pattern of the relative immune cells and cytokines/growth factors expression, from (Maruyama et al., 2020).*

As seen in **Figure 3**, each phase can be further divided into six sub-steps: hematoma, inflammation, soft and hard callus formation, remodeling and bone healing. After bone trauma, i.e., a fracture, in the inflammation phase immune cells such as polymorphonuclear neutrophils (PMNs), natural killer (NK) cells, mast cells and platelets are activated and then, secreted cytokines and chemokines recruit and activate monocytes and macrophages, which later play important roles in the process. The pro-inflammatory cytokines (IL-1β, IL6, TNFα) are essential signals during the early stages, since TNFα increases in the late repair phase and the other cytokines increase in the remodeling phase. The control of the expression of said biomarkers in the late stages of inflammation is critical to fracture repair (Maruyama et al., 2020).

However, there's evidence that the key pro-inflammatory cytokines (IL-1β and TNFα) have significant effects on the suppression of osteoblast development, both at the differentiation and proliferation levels. It is also known that they suppressed mineralization, ALP activity and mRNA expression for Col1a1, Runx2 and osterix, even at lower concentrations. These cytokines can have major consequences for

normal bone development and they are mainly responsible for reduced bone mass (Lacey et al., 2009).

As mentioned in section 1.1, some pathways are followed for bone proliferation and differentiation. These pathways could be affected by TNF-$\alpha$ and IL-1β promoting bone loss by activating osteoclastogenesis, and a decrease in mineral density by inhibiting osteoblastic differentiation and bone formation, which are suspected causes of low osteo-inductive efficacy of BMP-2 (Huang et al., 2014). On the other hand, a significant production of Nitric Oxide (NO) is a signal of possible early increased formation of bone and, in addition, an increase in the intracellular calcium concentration may lead to a decrease in cell proliferation (Preez et al., 2018).

## 1.2 Bone Loss

Aging population is becoming common among most countries. According to ENADID (Encuesta Nacional de la Dinámica Demográfica) 2018, in México there are 15.4 million people above age the of 60, which represent 12.3% of total population (INEGI, 2019). Among the most common orthopedic problems, requiring medical intervention, are bone fractures, particularly in the elderly. Half of fractures are related to osteoporosis and are present especially in individuals over the age of 55. This has a huge impact on health and quality of life, also considering the multi-billion-dollar cost to society due to direct and indirect costs (Gibon et al., 2016).

As seen in previous sections, bone undergoes continuous modelling and remodeling, and some factors can interfere with osteoblast function or osteoclasts activity. Osteopenia occurs when osteoclasts reach a level of hyperactivity or osteoblasts are insufficiently activated, so an imbalance between bone formation and bone resorption takes place. This imbalance can have both metabolic (osteomalacia) or endocrine (hyperparathyroidism or postmenopausal osteoporosis) origin, the latter affecting more than 50% of women over 60 years (**Figure 4**) (Redlich & Smolen, 2012).

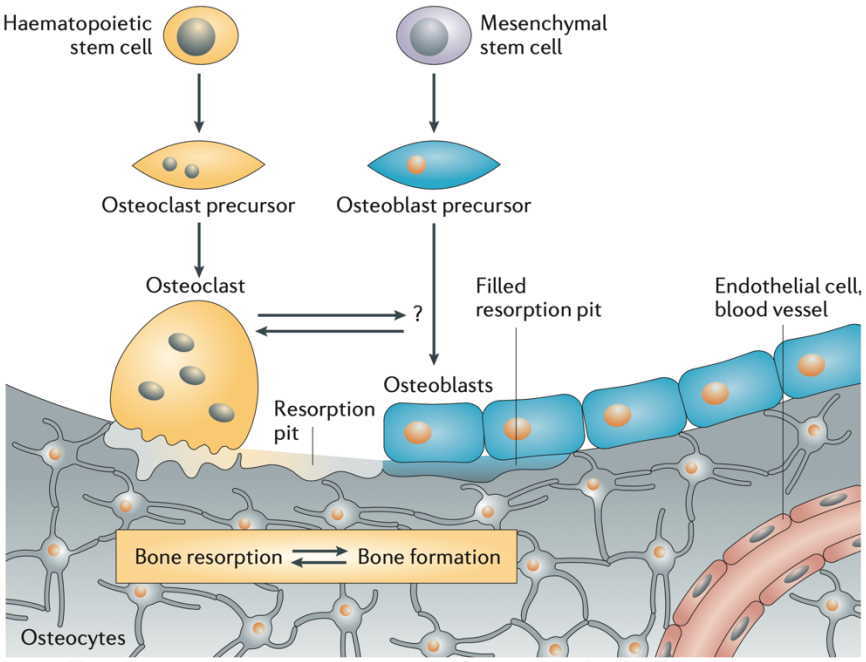


***Figure 4.*** *Maintenance of bone structure, from (Redlich & Smolen, 2012).*

It is also known that this imbalance is linked to various diseases such as chronic inflammation diseases with systemic osteoporosis, which increases fracture rates, causes excessive bone resorption and, subsequently, impaired bone formation (Redlich & Smolen, 2012). As seen in section 1.1.2, the degree of inflammatory response is linked to the extent of local and systemic bone loss. Several therapeutic interventions have been researched to effectively reduce inflammation, however they don't eliminate it, so bone loss continues (Redlich & Smolen, 2012). Thus, the need to evaluate current solutions and limitations, and develop new alternatives with therapeutic potential to treat bone loss.

### 1.2.1 Prosthesis systems

One of the most common solutions for bone loss are joint arthroplasties, with hip and knee being the most frequent. Joint arthroplasty began in the 19$^{th}$ century, evolving to a modern surgical procedure developed between 1950s- 1970s. Nowadays, the number of hip and knee replacements has significantly increased in most European countries (Vaz et al., 2017).

On the other hand, cementless fixation has also been studied for a period of evaluation over the last two decades in total hip arthroplasty. One of the most

important factors of this solution is the surface texture, since this influences the success rate of the procedure. The main types of surfaces used are porous and hydroxyapatite, but they keep showing bone loss afterwards, maintaining it as a main concern (Rahmy et al., 2004).

#### 1.2.1.1 Prosthetic Joint infection

Most arthroplasties successfully relieve pain and improve function. However, some of the most common complications that have arisen in some patients are loosening and infection. Loosening can occur between 10-20 years after joint replacement in a rate of 2-18% of prosthesis. On the other hand, infections occur in 2-3% of all primary joint replacements and in 5-8% of revision joint replacement (Vaz et al., 2017). Both complications require different treatments but they but represent a growing and substantial burden, especially with prosthetic joint infection (PJI), which could lead to lifelong suppressive antibiotic treatment in 45-52% of patients, requiring subsequently and constant revision of the implants (Lenguerrand et al., 2017).

In addition, infection is the most feared complication in total hip arthroplasty, since it is associated with more readmissions, longer length of stay and subsequent revisions, with an increased mortality risk within 1 year after revision for PJI (Gundtoft, 2017). On the other hand, a study made by Atallah, et al., 2018, concluded that major complications such as implant infection, implant loosening and intermedullary device breakage are rare in transfemoral bone-anchored prosthesis and occur in less frequency in individuals with press-fit implants. In addition, minor complications like soft tissue infections are more common and underreported in most articles (Atallah et al., 2018).

In total knee arthroplasty (TKA), PJI is the most common cause of failure. The overall risk of developing these infections depends on several factors, with the highest risk period during the first 2 years after the procedure, while there's ongoing soft tissue healing and postoperative inflammation is still present. Some surgical factors include the location of the arthroplasty, the potential for soft tissue healing or complications, and the potential for presence of subclinical infection. On the other hand, some patient factors increasing the rate of PJI include the presence of

comorbidities such as arthritis, diabetes mellitus, malignancy, chronic kidney disease, obesity, history of immunosuppression and difficult wound healing, along with smoking (Beam & Osmon, 2018).

In terms of cost, each PJI diagnosis have an annual cost of $566 million USD during 2009 and was expected to increase to $1.62 billion dollars during 2020. These costs depend on the treatment approach, including debridement, antibiotic therapy, among others (Beam & Osmon, 2018).

#### 1.2.1.2 Metal toxicity in prosthesis

Additional surgery related risks have arisen due to the use of metal-to-metal hinged prosthesis (Beam & Osmon, 2018). By using this material along with alloys, high quality plastic and polymer materials, long-lasting prostheses can be made, allowing the reconstruction of fractures or the replacement of painful, dysfunctional joints, enable patients to live a more fulfilling and active life. Nevertheless, these implants only last for 10-15 years leading to implant failure, loosening, infection (as previous mentioned) or high toxicity and side effects (Colic & Sedmak, 2016).

Despite improvements made in the past decades, wear and corrosion products associated with the metal components may result in adverse reactions and toxicity, with their pertinent side effects such as liver and kidney disfunction, and neurodegenerative diseases like Parkinson's, dementia, dialysis encephalopathy and Alzheimer's. This is mainly for the effect of Cobalt-Chromium-Molybdenum (CoCrMo) wear micro- and nano-particles, ions of different valences and oxides (Bijukumar et al., 2018).

On the other hand, a case reported by Jelsma, et al., 2020, revealed that metal-on-metal hip arthroplasty lead to high metal ion concentration which could result in cardiotoxicity, thyroid toxicity and/or neuro-ocular toxicity, including a high risk of the development of neurodegenerative diseases like Creutzfeldt-Jakob, with neurological symptoms revealing 7 years later (Jelsma et al., 2020). Several other cases have been reported (Biglia et al., 2020; Ho et al., 2017; Moniz et al., 2017) among others, where they have described the previously mentioned symptoms and pathologies derived from metal prosthesis toxicity.

# 2. Nanofiber scaffolds

Nanofibers have emerged as a potential novel platform due to its physicochemical properties for healthcare application. Tissue engineering has emerged as an alternative approach with the aim of repairing or reconstructing damaged or diseased tissues and organs with polymeric biomaterials, cells and growth factors, both individually and in combination. This is of great significance since it represent a huge role in cell migration, attachment and proliferation (Heidari et al., 2019). Their advantages rely in their high specific surface area-to-volume and porosity, and, in addition, their peculiar assembly allow cell accommodation, nutrient infiltration, gas exchange, waste excretion, high drug release rate and stable structure. Different strategies have been reported to enhance physical and mechanical characteristics of nanofibers and increase production yield rate (Gautam, Dinda & Mishra, 2013; Jin et al., 2013; Mehetre, et al., 2015).

## 2.1 Methods for nanofiber fabrication

Several techniques for the production of nanofibers have been developed in order to enhance production time, to include more and better materials and to lower costs, among other characteristics (Farokhi, M., et al., 2020; Meraz-Dávila, S., et al., 2021; Rim, N. G., et al., 2013; Wang, H., et al., 2013; Zamani, M., et al., 2013). Some of the latest techniques that are most commonly used when creating products based in nanofibers, such as electrospinning, forcespinning, solution blow spinning and $CO_2$ laser supersonic drawing.

One of the most widely used technique for the production of nanofibers is electrospinning (E-spinning), since it offers a number of advantages such as easy control for fiber production parameters and an adequate fiber properties and morphology (Thakkar & Misra, 2017). In addition, electrospinning offers a versatile, simple and cost-effective method that has provided a promising opportunity to fabricate nanostructured scaffolds that are capable of mimicking the fibrillar structure of natural ECM (Heidari et al., 2019).

### 2.1.1 Electrospinning

One of the most widely used technique over the last decade for the production of nanofibers is electrospinning. It has offered a number of advantages such as easy control for fiber diameter, surface characteristics, morphology, porosity, and the possibility of getting a fiber with measurements within the nanorange (around 10 nm-2μm) (Thakkar & Misra, 2017).

On the other hand, since the basic set up for the electrospinning is rather simple, it provides other advantages like high production rate with low costs, making it accessible to almost every laboratory. The basic components include a high voltage power supply, a syringe pump, a spinneret and a conductive collector (**Figure 5**). This technology allows the development of a wide variety of electrospun membranes, opening the possibility of many applications in various fields (Bavatharani et al., 2021; Xue et al., 2019).

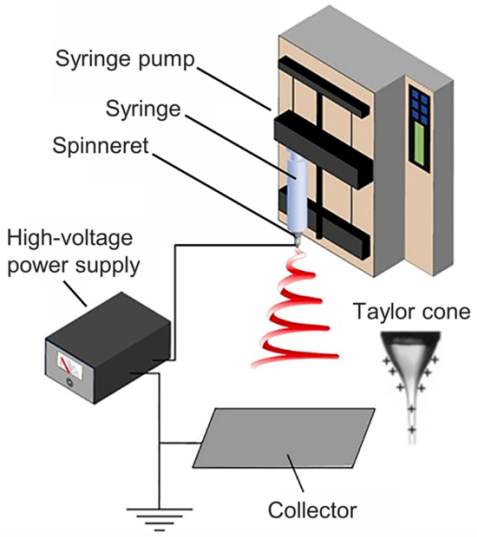


***Figure 5.*** *Basic Electrospinning Set Up, from Xue et al. (2019).*

The principle of electrospinning involves an electrohydrodynamic process, during which a liquid droplet is electrified to generate a jet, followed by stretching and elongation to generate fibers (Xue et al., 2019). More in detail, a polymer solution is pumped over a spinneret to shape a pendant droplet, when the electrostatic forces generated by the electric field overcome the surface tension of the solution, a Taylor cone will be formed at the syringe needle tip. Subsequently, a liquid jet will be formed, and it will travel in the track of the counter electrode. Through

the drive of the liquid jet, solvent evaporation occurs, whips are elongated, resulting in the deposition of continuous electrospun nanofibers in the collector (Peng & Ilango, 2020; Zaarour et al., 2020).

Surface morphology and general physical characteristics of the prepared nanofibers can be clearly affected by several parameters such as type of polymer or solvent used, solvent concentration: low concentration can lead to major defects in the final product, while high concentration can increase fiber diameter; as well as polymer solution parameters such as viscosity, surface tension, conductivity, polymer molecular weight, solvent volatility, dielectric constant.

Other parameters that affect are the type of spinneret and the tip-to-collector distance, where increased distance produces coarser fibers and reduced distances can cause defects in the nanofiber mesh. In addition, feeding rate, deposition time, evaporation rate, surface charge, ionization field and environmental conditions, such as temperature and humidity, are other factors that affect nanofiber's morphology (Havlíček et al., 2020; Zhao et al., 2008). A large variety of polymers are used to create electrospun nanofibers as candidates for the design of scaffolds for bone regeneration (Fang et al., 2010).

#### 2.1.1.1 Use of polymers for the fabrication of electrospun nanofibers

Polymers are considered as excellent materials for the fabrication of electrospun scaffolds due to its versatile chemical, biological, structural and mechanical properties, enabling scaffolds to support tissue regeneration and be reabsorbed, they have been used for health care applications since they are considered the most suitable class of materials due to its properties such as histocompatibility, biodegradability, lack of antigenicity and biocompatibility (Behere et al., 2020; Uppal et al., 2011) (Behere et al., 2020).

Natural polymers are suitable for this application thanks to its bioactivity, biocompatibility and its ability to not initiate immunological response (Morris et al., 2017). On the other hand, synthetic polymers add important characteristics such as slow rate of degradation, mechanical strength and porosity (Liu et al., 2013). A combination of both types of polymers helps to develop a complete functional

scaffold with both bioactivity and biocompatibility and good mechanical strength (Behere et al., 2020).

Among the most important synthetic polymers used for these applications, are poly($\varepsilon$-caprolactone) (PCL) and poly(lactic acid) (PLA) due to its rigidity, and because of its biocompatibility, which makes them suitable to produce composites with osteoconductive properties for bone regeneration (Mohandesnezhad et al., 2020).

In particular, PCL, a synthetic polyester polymer, is known for its higher flexibility in comparison with other polymers, however it has considerably slow biodegradation rate, which is carried by hydrolysis of its ester linkages in physiological conditions rate and low hydrophobicity (Fang et al., 2010; Mohandesnezhad et al., 2020; Wang et al., 2013). On the other hand, PLA, a rigid aliphatic synthetic polyester, is known for its great biocompatibility in vitro and it has proven that it doesn't accumulate in vital organs. However, its biomechanical strength is a limitation in several applications since it is affected by several parameters such as polymer ratio, molecular weight, crystallinity, that influences viscosity, porosity, structure and degradation rate (Fang et al., 2010; Mohandesnezhad et al., 2020; Wang et al., 2013).

It is known that a biopolymer nanofiber scaffold would be an ideal material used in health care applications since it is enhanced with properties such as greater water retention capacity, it presents fewer immunogenic reactions and its surface is soft to the touch, so it won't chafe the wounds or the area where it is applied (Uppal et al., 2011). A blend of polymers is expected to have enhanced properties such as flexibility, and excellent biodegradability, and the addition of natural herbal extracts could improve its bioactivity, roughness and even osteoconductivity, among other properties (Fang et al., 2010).

#### 2.1.1.2 Natural herbal extract incorporation

Given the beneficial properties of bioactive compounds there has been an increasing interest for incorporating them into several delivery systems, since they sometimes present low bioavailability or are needed to have a more controlled release on different surfaces. The incorporation of active compounds into

appropriate carries may enhance their properties due to characteristics such as higher surface area and enhanced mechanical properties (Surendhiran, *et al*., 2020).

Herbal bioactive compounds from plants have been used since ancient times, however, they have recently gained special interest. These compounds are known for its beneficial properties and healing performance of their secondary metabolites for the treatment of diseases with lower side effects compared with synthetic drugs. Natural extracts are considered as a viable alternative for new applications due to its wide variety of chemical compounds and biological activities (Hosseinzadeh et al., 2015).

Some authors have studied different plants rich in phenolic compounds such as *Lawsonia inermis* L (Henna) (Adeli-Sardou et al., 2019), *Centella asiatica* (Yao et al., 2017), *Chamomilla recutita* (L.) (Motealleh et al., 2014), *Stryphnodendron adstringens* (de Oliveira Mori, et al., 2014) to validate its incorporation to fibers production (**Table 2**). Plant bioactive compounds are the key factors for the extract's therapeutic properties such as hypoglycemic, antidiabetic, antioxidant, antimicrobial, anti-inflammatory, anticarcinogenic, among others. Fabricant and Farnsworth (2001) point that by analyzing and using natural extracts from plants as medicine is possible to achieve different clinical therapeutic goals such as isolate bioactive compounds for a direct use as a drug, synthesize novel chemical structures from a known bioactive compound and use of bioactive compounds as pharmacological tools.

***Table 2****. Natural Herbal Extracts Incorporated to Polymer Nanofibers by electrospinning (Part 1).*

| Herbal Component | Polymer | Properties | Reference |
|---|---|---|---|
| *Curcuma comosa* Roxb. Extract | Gelatin | Antioxidant, anti-tyrosinase and anti-bacterial activities | Chiu, C., et al. 2019 |
| *Lithospermi radix* extract | Gelatin/ Chitosan/ PVA | Non-immunogenicity, antibacterial, tissue regeneration, anti-inflammatory, anti-apoptosis | Yao, C., et al. 2018 |
| Pomegranate (*Punica granatum)* peel extract | Chitosan/ Polyethylene oxide (PEO) | Antioxidant, anti-diabetic, anti-hypersensitive, anti-inflammatory, antiviral, anti-bacterial | Surendhiran, D. et al, 2020 |
| *Aloe vera* extract | Chitosan/ Polyethylene oxide (PEO) | Wound healing, anti-inflammatory, strenghtening of immune system, anti-carcinogenic, anti-diabetic, antioxidant. | [99] Nikbakht, M., et al. 2020 |
| *Artemisia* extract | Chitosan | Antimicrobial | [100] Rezaei, M., et al. 2019 |
| *Urtica dioica* L. extract | PCL | Antimicrobial | [101] Erbay, E., et al. 2017 |
| *Eleaeagnus angustifolia extract* | PEG-PCL-PEG | Antinociceptive, anti-inflammatory, antibacterial, antioxidant | [102] Hokmabad, V., et al. 2018 |
| Date palm fruit extract | PLA | Polyphenolic activity, antioxidant, anti-diabetic, anti-carcinogenic, antibacterial | [103] Zadeh, K., et al. 2019 |

**Table 2.** Natural Herbal Extracts Incorporated to Polymer Nanofibers by electrospinning (Part 2).

| Herbal Component | Polymer | Properties | Reference |
|---|---|---|---|
| *Lallemantia royleana* extract | PVA | Antioxidant, polyphenolic and antimicrobial activities | [105] Rezaeinia, H., et al. 2020 |
| *Lallemantia royleana* extract | PVA | Antioxidant, polyphenolic and antimicrobial activities | [105] Rezaeinia, H., et al. 2020 |
| *Aloe vera* extract | Chitosan/ Polyethylene oxide (PEO) | Wound healing, anti-inflammatory, strenghtening of immune system, anti-carcinogenic, anti-diabetic, antioxidant. | [99] Nikbakht, M., et al. 2020 |
| *Artemisia* extract | Chitosan | Antimicrobial | [100] Rezaei, M., et al. 2019 |
| *Urtica dioica* L. extract | PCL | Antimicrobial | [101] Erbay, E., et al. 2017 |
| *Eleaeagnus angustifolia extract* | PEG-PCL-PEG | Antinociceptive, anti-inflammatory, antibacterial, antioxidant | [102] Hokmabad, V., et al. 2018 |
| Date palm fruit extract | PLA | Polyphenolic activity, antioxidant, anti-diabetic, anti-carcinogenic, antibacterial | [103] Zadeh, K., et al. 2019 |
| *Lallemantia royleana* extract | PVA | Antioxidant, polyphenolic and antimicrobial activities | [105] Rezaeinia, H., et al. 2020 |
| *Lallemantia royleana* extract | PVA | Antioxidant, polyphenolic and antimicrobial activities | [105] Rezaeinia, H., et al. 2020 |
| Grape Seed (*Vitis vinifera L.*) extract | PVA | Antioxidant | [106] Faki, R. et al. 2019 |
| *Juniperus chinensis* | PVA | Antibacterial, antifungal, antioxidant | [107] Kim, J., et al. 2016 |
| Lanasol from *Rhodomela confervoides* | PMMA/ PEO | Antimicrobial | [108] Andersson, R., et al. 2014 |

**Table 2.** Natural Herbal Extracts Incorporated to Polymer Nanofibers (Part 3).

| Herbal Component | Polymer | Properties | Reference |
|---|---|---|---|
| Tea tree oil extract (Melaleuca alternifolia)/ Pomegranate peel extract | HP-ß-Cyclodextrin | Antioxidant, anti-inflammatory, antiseptic and antimicrobial | Kalouta, K., et al. 2019 |
| *Moringa oleifera* leaf extract | Polyacrylonitrile | Antimicrobial, antiproliferative, antioxidant, polyphenolic activity | Fayemi, E., et al. 2018 |
| Resveratrol Veri-TeTM | Zein from maize | Antioxidant, anti-cancer, tissue engineering, barrier, prevention of moisture loss and color retention | Leena, M., *et al*., 2020 |
| *Momordica charantia* fruit extract | Zein/gelatin | Antioxidant | Torkamani, A., *et al*., 2018 |

Several plants have shown therapeutic effects, due to this they have been incorporated to delivery systems to enhance properties such as stability, liberation, among others. The use of natural materials in electrospinning is increasing, with the most important being alginates, cellulose, dextran, chitosan, among others (Thomas et al., 2012). An example of a matrix that provides bioactive compounds suitable for this application is *Opuntia ficus-indica* (OFI), which is an important medicinal plant best known for its beneficial health effects, including anti-inflammatory and wound-healing, immunomodulatory, antiviral, antioxidant, among others (Santos-Zea et al., 2011).

# 3. Importance of *Opuntia Ficus-Indica L. Mill* as a major crop in México

## 3.1 National distribution and added value

México, especially center and south, is known as one of the main places of distribution and domestication of *Opuntia ficus-indica L. Mill* in America (Vanegas-Rico, Lomeli-Flores, Rodríguez-Leyva, Mora-Aguilera, & Valdez, 2010). *Opuntia* is a crop species, known as a major product in the agricultural economy of modern México, and one of the most important, ideal for arid regimes due to its extremely efficiency at converting water into biomass (Griffith, 2004), and recognized for its use in numerous ways as food or fodder (Kiesling, 1995). Also, the lack of a well-defined standard for varieties, has led to the development of clonal populations in producer countries, which are mostly distinguished based on some morphological features of the fruits and its cladodes (Chiteva & Wairagu, 2013). This plant has been traditionally used as a medicinal plant to treat a variety of diseases, particularly diabetes and hypercholesterolemia, and has been related to other health effects such as anti-inflammatory and wound-healing, antigenotoxic, neuroprotective, hypotensive, immunomodulatory, antiviral and antioxidant to combat oxidative stress (Santos-Zea, Gutiérrez-Uribe, & Serna-Saldivar, 2011), all which has been attributed to its chemical composition, which will be next described.

## 3.2 Chemical composition of *Opuntia ficus-indica L. Mill*

*Opuntia ficus-indica L. Mill* has shallow root systems that enables it to accumulate elements, which has made it suitable for nutraceutical and functional foods applications by embracing its essential ingredients composition (Chiteva & Wairagu, 2013). It presents a high content of water and a proportion of dietary fiber, lipids, proteins and calcium, and other components such as antioxidants like ascorbic acid, ß-carotenes, lutein and xanthophylls (López-Cervantes, Sánchez-Machado, Campas-Baypoli, & Bueno-Solano, 2011). Mainly, its beneficial effects have been attributed to its dietary fiber and to its phytochemicals such as phenolic acids, flavonoids, carotenoids and vitamins (Santos-Zea et al., 2011). It is a major

source of polysaccharides, which are abundant in cladode extracts and endowed with antidiabetic and antiglycation effects (El-mostafa et al., 2014). Some researchers have studied the proximal content of some molecules and activities as shown in **Table 3**.

***Table 3**. Proximate composition of Opuntia ficus-indica (L.) Mill fruits with spines (Chiteva & Wairagu, 2013).*

| Sample | Moisture content (%) | Ash (%) | Vitamin C (mg/100 g) | Protein (%) | Crude fat (%) | Crude fiber (%) | Calorific Value (Kcal/g) | Sugars (NR) (%) | Carbohydrates (%) |
|---|---|---|---|---|---|---|---|---|---|
| **Composition** | 87.07± 0.86 | 4.03 ± 0.52 | 5.17 ± 0.06 | 1.03 ± 0.06 | 0.4 ± 0 | 1.37 ± 0.06 | 3.77 ± 0.06 | 59.4 ± 0.1 | 92.57 ± 0.99 |

Consequently, there has been a growing interest in the use of cactus as a nutraceutical supplement in various processed foods and several other applications, which is why there's been the strong need to create novel delivery systems for these compounds, for example in flours (Santos-Zea et al., 2011).

### 3.2.1 Anti-inflammatory compounds in *Opuntia ficus-indica*

OFI has been studied for its anti-inflammatory effects, which have been attributed to different phytochemicals such as its most abundant flavonoids, the isorhamnetin glycosides. Several studies have shown that OFI extract and its isorhamnetin glycosides suppress NO production *in vitro* without affecting cell viability, significantly inhibits TNF-α production, placing it as a suitable natural compound for the development of new anti-inflammatory ingredients (Antunes-Ricardo, Gutiérrez-Uribe, López-Pacheco, et al., 2015; Antunes-Ricardo, Gutiérrez-Uribe, Martínez-Vitela, et al., 2015). There is also some evidence that OFI is an important source of calcium and may have potential for applications in the prevention and treatment of diseases associated with calcium deficiency (Contreras-Padilla et al., 2011).

### 3.2.2 Phytochemicals on bone proliferation

Interest has risen in the prevention and treatment of bone loss related diseases with naturally derived compounds. Specifically, focus has been put in polyphenols since they affect bone metabolism by anti-inflammatory actions, suppression of osteoclastogenesis and activation of osteoblastogenesis via different bone related pathways (Austermann et al., 2019). Recently, most research has focused on flavonoids' possible benefits on bone health, concretely flavonols, of which several *in vitro* e *in vivo* studies have been made. These studies have shown that the flavonols quercetin and kaempferol are able to counteract the bone deleterious effect of estrogen deficiency occurring during menopause; and their aglycones exert a potent inhibitory effect on osteoclastic bone resorption and apoptosis in rabbit long bone osteoclast model (Habauzit & Horcajada, 2008).

On the other hand, some authors have reported the effect of isorhamnetin in women postmenopausal osteoporosis (PMOP), where it promotes osteoprotegerin (OPG) expression in bine tissue, inhibits RANK/RANKL signaling pathway activation, regulating the function of osteoblast and osteoclasts, inhibiting the destruction of bone and improving bone microstructural damage in ovariectomized rats (Gong et al., 2020). Another research made by Jin et al., (2013) conclude that it may contribute to blockade of the host-destructive processes mediated by IL-6, contributing to an efficient treatment of inflammatory periodontal disease (Jin et al., 2013).

# 2. Materials and Methods

The present design of experiments (**Figure 6**) consisted in the elaboration of OFI flour-enhanced electrospun nanofibers. Firstly, a prelaminar test was carried in order to define the parameters for elaboration of the electrospun nanofibers, followed by the definition of flour:polymer ratio for its addition to the electrospun nanofibers. Next, the fibers were characterized in order to know its chemical and morphological composition, and several properties as swelling capacity and degradation rate, as well as its release kinetics. Finally, biological assays *in vitro* were carried: cell cytotoxicity, calcium deposition.

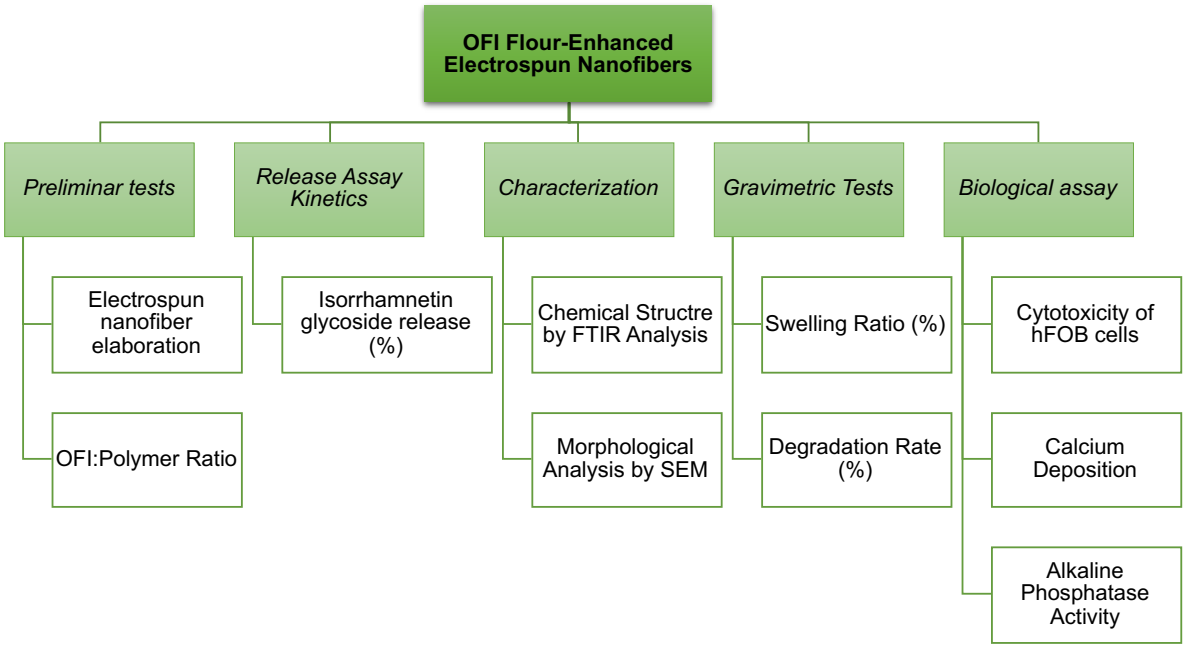


***Figure 6**. Experimental Strategy Diagram.*

## 2.1 Chemicals and Reagents

Polycaprolactone (PCL), Methanol solution were obtained from DEQ (Monterrey, N.L, México), Acetonitrile (ACN) was obtained from J.T. Chemical Co. (Phillipsburg, NJ, USA), Isorhamnetin standard was purchased from Indofine Chemical Co. Inc (Hillsborough, NJ, USA). HPLC grade water and methanol were obtained from VWR international LLC (West Chester, PA, USA). Phosphate saline solution (PBS) pH 7.4

(1x) was acquired from Gibco Laboratories (Grand Island. NY, USA), Celltiter96®AQueous One Solution Cell Proliferation Assays from Promega (Madison, WI, USA).

## 2.2 Biological Material

The *O. ficus-indica (L.)* Mill plant was harvested in the region of Montemorelos, Nuevo León, México and the taxonomic identification was performed at the School of Agronomy of Universidad Autónoma del Nuevo León (UANL), México. Cladodes were harvested at 7 months and processed into flour, as reported by Antunes-Ricardo et al. (2017). The flour was packaged in dark bags and stored at -20°C until extraction.

## 2.3 Determination of process parameters of nanofiber elaboration by electrospinning.

Three solutions with different polymers (PCL, PMMA, PLA) at 30% w/v were made, dissolved in chloroform with 4h of agitation at 65ºC as established in preliminary tests. After agitation, each solution was electrospun (**Figure 7**) with the following parameters: distance of 15 cm, flow rate of 1 mL/h, and a voltage of 20 kV (Rabiatul et al., 2015; Rezaeinia et al., 2020; Zadeh et al., 2019; D. Zhang et al., 2019). After one hour, the fibers were collected and were left to dry for 24 hrs. After dryness, the fibers were weighted and prepared for extraction.

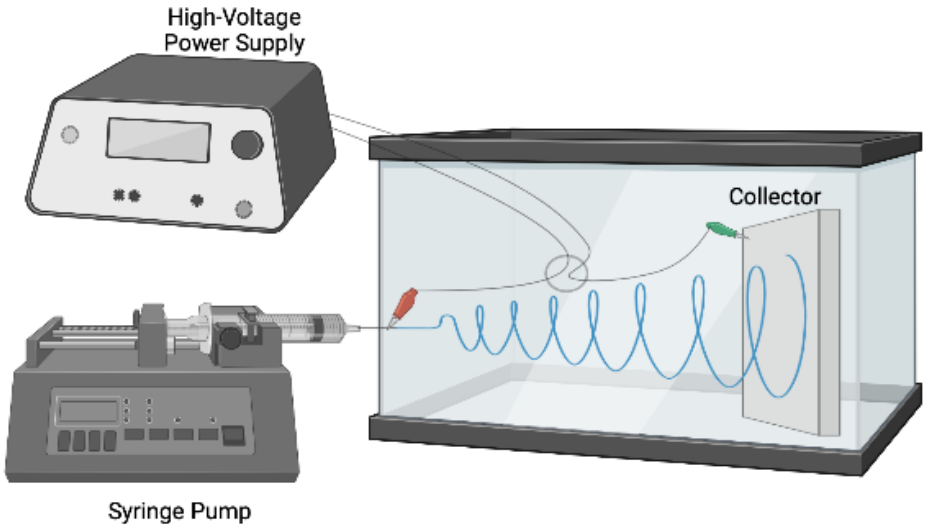


***Figure 7**. Electrospinning Set up.*

## 2.4 Addition of OFI flour to electrospun nanofibers solution.

Four different percentages (10%, 30%, 50% and 70% w/w) of OFI flour were added to polymer solution and were electrospun under the following parameters: distance of 15 cm, flow rate of 1 mL/h, and a voltage of 20 kV. In addition, control fibers without OFI flour were made under the same conditions (**Figure 8**). After two hours, the fibers were collected and were left to dry for 24 hrs. After dryness, the fibers were weighted and prepared for extraction.

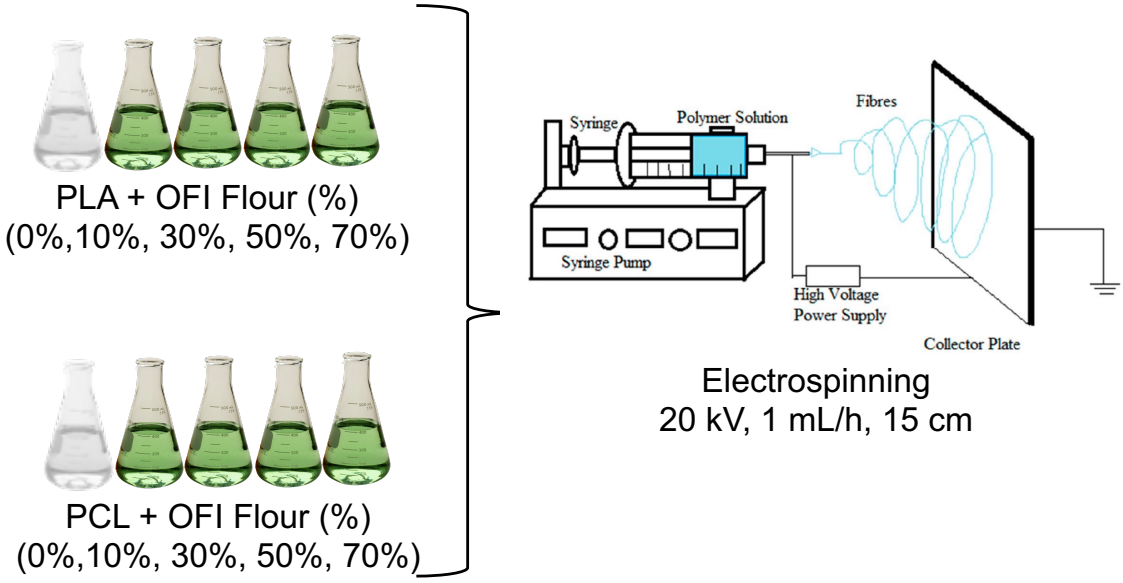


***Figure 8**. Opuntia ficus-indica flour addition to polymer solution.*

## 2.5 Determination of isorhamnetin glycoside content by HPLC-UV

Once the fibers were weighted, they were extracted in a MeOH 80% (1:10 w/v) solution, they were vortexed and then centrifuged at 10 000g at 4ºC for 15 min. After this, they were dried in vacuum, and resuspended a MeOH 20% solution. Next, the fibers were sonicated for 1 min and then centrifuged 15 min at 10 000g at 4ºC. Promptly they were transferred to vials for its quantification as milligrams of isorhamnetin equivalents per g of nanofiber using an isorhamnetin standard (Sigma, St. Louis, MO.). Quantification was performed using a high-pressure liquid chromatograph with UV detector (HPLC-UV) (Agilent 1100 Series Santa Clara, CA, USA) and chromatograms were obtained at 365 nm. Separation was carried by an analytical Zorbax Eclipse XDB-C18 (4.6 x 150 mm, 5µm) column operating at temperature of 25ºC with a flow rate of 0.450mL/min. The mobile phase used was

(A) water with 0.1% formic acid (Sigma, St. Louis, MO.) and (B) methanol (Antunes-Ricardo et al., 2018). The isorhamnetin glycoside separation was achieved using a solvent gradient with 35% of B for the first 5 minutes, next it was increased to 60% until 20 min, and further increased to 90% up to 25 min, decreasing to 0% until the 30 min. Isorhamnetin glycosides were quantified as micrograms of isorhamnetin (Sigma, St. Louis, MO) equivalents (µg IsoEq) by each 1 gram of fiber.

## 2.6 Nanofiber Chemical and Morphological Characterization

The morphology of the PCL and PLA electrospun nanofibers was observed using Scanning Electron Microscopy (SEM) (JEOL JSM6360LV, UNAM, CDMX). The specimens were sputter-coated with gold and analyzed at an accelerating voltage between 0.5 and 30 kV and in an amplification range from 500X to 3000X.

On the other hand, chemical composition of the nanofibers was observed using Fourier Transformed Infrared (FTIR) spectroscopy equipped with an attenuated total reflection accessory with a SeZn crystal (PerkinElmer, Inc. Waltham, MA). The nanofibers were used directly in the ATR-FTIR in order to confirm isorhamnetin glycoside concentration. The spectra were obtained within the wave number range of 550-4000 $cm^{-1}$, with a $4cm^{-1}$ resolution, scan number: 8, force gauge > 90 Gauge and %T units (Jiménez-Rodríguez et al., 2021).

## 2.7 Release Analysis of Isorhamnetin Glycosides

The released amount of isorhamnetin glycosides was determined by suspending 2 $cm^2$ of nanofibers in 1.5 mL of PBS pH 7.4. The nanofibers were incubated at 37°C while shaking at 150 rpm in an Incubating Orbital Shaker (VWR®, Model 35009I, Radnor, PA, USA). At 2, 4, 8, 12, 24 and 48h, 300 µL of the supernatant were removed from the medium and then the same volume of PBS was added. The collected samples were analyzed using HPLC-UV (Agilent 1100 Series Santa Clara, CA, USA) following the previously described method (*section 2.5*). The cumulative isorhamnetin glycosides release percentage was calculated according to the following equation:

$$\text{Release } (\%) = \left( \frac{[\text{Released Isorhamnetin Eq. } (\mu g)]}{[\text{Total Isorhamnetin Eq. } (\mu g)]} \right) * 100$$

the percentage of drug released was expressed in isorhamnetin equivalents (%) and plotted against time.

## 2.8 Biodegradation Rate

This assessment was carried according to Zhang *et al.*, 2019. The electrospun nanofibers were weighted and each mass was recorded (W1). Then, they were immersed in phosphate buffer (PBS, pH 7.4, 37ºC) mixed with protease K solution (6 µg/mL), in a ratio of 1:1000 w/w nanofiber to solution while shaking at 150 rpm. Samples were extracted at 24h and 48h and then washed with distilled water and dried in 37ºC oven for 4 days and weighted again (W2). Degradation rate was calculated as follows:

$$Degradation\ rate\ (\%) = \frac{(W1 - W2)}{W1} \times 100$$

## 2.9 Swelling Rate

Swelling Rate assay was performed according to the reported by Ko *et al.*, 2010. Each nanofiber was weighted (W1) and then immersed in phosphate buffer solution (PBS, pH 7.4) at room temperature for 24h. Water excess was removed from the swollen nanofibers and then, they were weighted immediately (W2). Swelling ratio was calculated as follows:

$$Swelling\ Ratio\ (\%) = \frac{W2 - W1}{W1} \times\ 100$$

## 2.10 Cell culture

The conditionally immortalized human fetal osteoblastic cell line (hFOB) cell lines were obtained from the American Type Culture Collection (ATCC) (Manassas, VA). Cells were cultured in petri plates with Dulbecco's Modified Eagle Medium (DMEM-F12), supplemented with phosphate buffer saline (PBS) at pH 7.4, 0.25% trypsin EDTA(1X), Penicillin (10000 Units/mL)-Streptomycin (1000 µg/mL) solution and 10% fetal bovine serum (FBS), purchased from GIBCO®/Life Technologies (Grand Island, NY). They were incubated at 37ºC and 5% of $CO_2$.

### 2.10.1Cell viability

Cell viability of hFOB cells in presence of PCL and PLA nanofibers loaded with isorhamnetin glycosides was performed using CellTiter96® Aqueous One Solution Cell Proliferation Assay (Promega, Madison, WI). Cells were seeded in a 96 well plates at a density of $5x10^5$ cells/mL. Initially, nanofibers were cut into circular discs (7mm) and exposed to UV radiation on both sides, under laminar flow hood for 1 h to ensure sterilization. After 24 h of seeding, nanofibers were added on the cells in each well. Then, after 24 and 48 h of incubation, 100 µL of each well were transferred to a new well plate, and it was measured using 10 µL of CellTiter96 per well, incubating during 45 min at 37°C. Absorbance of supernatants was measured at 490 nm with a microplate reader (Synergy HT, BioTec, Winooski, Vermont, USA). Cell viability was obtained by dividing the absorbance of cells with OFI nanofiber by the absorbance of control cells.

In order to identify cell organelles a Hoesch Tinction assay was carried, for this, medium was washed with PBS. Cells were fixed with ethanol, then Hoesch dye was added. Cells were washed again with PBS and blue fluorescence was observed. Morphological changes between day 1 and day 7 were shown, along with cellular distribution in the scaffold (Ramírez-Fernández et al., 2013)

### 2.10.2 hFOB Cell differentiation and maturation

Cell differentiation was carried using a differentiation hFOB medium (DMEM-F12), as previously described (section 2.10). The assay of Alkaline Phosphatase (ALP) Activity was carried in order to evaluate the hFOB cells maturation. For this, the cells were seeded in a 96 well plates at a density of 10000 cells per well, and they were grown to 80% confluence at 37ºC for 24h. Subsequently, cells were cultured in differentiation medium for 6 days at 37ºC, replacing the medium every 3 days. ALP activity was measured using the colorimetric assay of the yellow nitrophenol, which converts from nitrophenyl catalyzed by the ALP enzyme at pH 9.8. The cells were washed three times with PBS, incubated with 100µL trypsin, and then the cell suspension was lysed by adding Triton X-100 lysis for 30 minutes, and then centrifugated at 15 000 g for 5 minutes to collect supernatants for ALP analysis.

Optical density value of each well was detected by microplate reader at 405 nm (Hassanajili et al., 2019; Lu & Zhao, 2018; Sabokbar et al., 1994).

### 2.10.3 Calcium Deposition

Under the same conditions previously described (*see section 2.10.2*), sterilized nanofibers were added on the cells in each well. Then, after a differentiation time of 6 days, cell medium was discarded and cells were washed with PBS and incubated with 2μM Calcein-AM in PBS at room temperature, for 30 minutes. After incubation, images were taken at random points per well by fluorescence microscopy at 495 nm (Eren et al., 2018).

## 2.11 Statistical Analysis

Experiments were performed at least by triplicate and the results were analyzed with Minitab LLC software (Pennsylvania State University, University Park, PA, USA) using ANOVA followed by Tukey's HSD tests. For each data set, $p<0.05$ was considered statically significant. The data was expressed as mean $\pm$ standard deviation.

# 3. Results and Discussion

## 3.1 Determination of Process Parameters of Nanofiber Elaboration by Electrospinning

Process parameters were stablished and adjusted according to (Rabiatul et al., 2015; Rezaeinia et al., 2020; Zadeh et al., 2019; Y. Zhang et al., 2008), depending on polymer concentration, desired width, and in line with the qualitative characteristics expected. PCL, PMMA, and PLA electrospun nanofibers were obtained, both control (0% OFI flour) and with OFI flour added (**Figure 9**).


***Figure 9.*** *Polycaprolactone (PCL), polymethylmethacrylate (PMMA), polylactic acid (PLA) nanofiber mesh obtained from electrospinning with and without Opuntia ficus-indica (OFI) flour at 30% w/v, 15cm, 1mL/h, 20kV.*

When recovering the polymer and polymer-OFI flour nanofibers (**Figure 9**) it was observed that the best qualitative (fiber-like) characteristics were obtained from PLA, followed by PCL, since they were forming a uniform mesh that was easy to recover entirely and showed strength. On the other hand, the recovery of PMMA and PMMA OFI flour was hard to achieve completely, since it showed an uneven surface

that, at contact, decomposed into a powder that didn't have the desirable fiber-like characteristics and, since it broke down, it was discarded.

## 3.2 Addition of OFI Flour to Electrospun Nanofibers' Solution

It was possible to develop electrospun nanofiber's mesh with the addition of different percentages of OFI flour (0%, 10%, 30%, 50% and 70% w/w). All PCL fibers were distinguished because of their porous surface appearance, while PLA fibers showed a smoother surface appearance, however, while increasing the OFI flour content, some lumps started accumulating on the surface (**Figure 10**). On the other hand, on both fibers, it was notable an increased green color directly proportional to the OFI flour content. Particularly, after visual inspection, the PLA electrospun nanofiber mesh appeared to be thinner in comparison to the PCL electrospun nanofiber mesh, indistinctively of the OFI flour content and under the same production conditions.

Previous research has proven that electrospinning versatility in generating nanofibers with different composition is dependent on polymer concentration, solvent, solvent ratio, flow rate, distance to collector and voltage, therefore, changing these parameters can affect the appearance and molecular structure, hence, viscosity, porosity, degradation and swelling rate of the fibers (Herrero-Herrero et al., 2018; Mohandesnezhad et al., 2020).

On the other hand, the PLA electrospun nanofiber mesh had more adherence and movements by itself when in contact with different surfaces, while in PCL this effect wasn't present. Hence, the PLA electrospun nanofiber mesh appeared to be more electrically charged than the PCL electrospun nanofiber mesh. PLA is known by its high resistivity and its tendency towards electric polarization and static electricity. Furthermore, PLA in films behaves like a typical dielectric with a small transient current that depends on the intensity of a direct current field, like that imposed by the electrospinning process. Higher voltage leads to a higher transient current, that decreases over time due to a slow dipole polarization which is possible in the PLA fibers on account of its polar groups (carbonyl groups) (Urbaniak-Domagala, 2013).

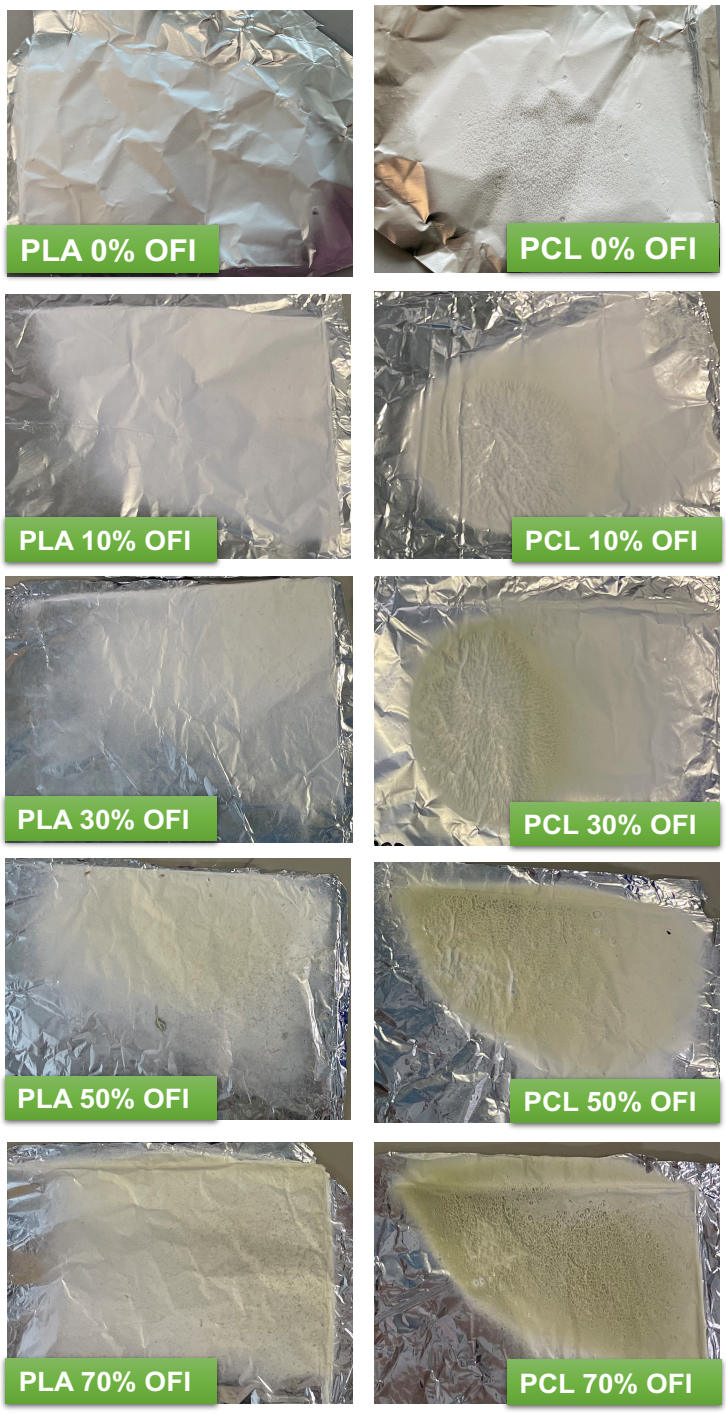


***Figure 10.*** *Polylactic acid (PLA) and polycaprolactone (PCL) electrospun nanofibers enhanced with 0%, 10%, 30%, 50% and 70% w/w Opuntia ficus-indica (OFI) flour.*

## 3.3 Determination of Isorhamnetin Glycosides Content by Semipreparative HPLC-UV

Isorhamnetin glycosides extracted from the PLA and PCL electrospun nanofiber were detected in a retention time range between 18-25 min (**Figure 11**). The isorhamnetin glycosides detected were: isorhamnetin glucosyl rhamnosyl rhamnoside (IG1), isorhamnetin glucosyl rhamnosyl pentoside (IG2), isorhamnetin glucosyl rhamnosyl methylpentoside (IG3), isorhamnetin glucosyl pentoside (IG4) and isorhamnetin glucosyl rhamnoside (IG5) (**Table 4**). These glycosides have been previously reported in OFI flour (Antunes-Ricardo et al., 2017, 2018; Santos-Zea et al., 2011).

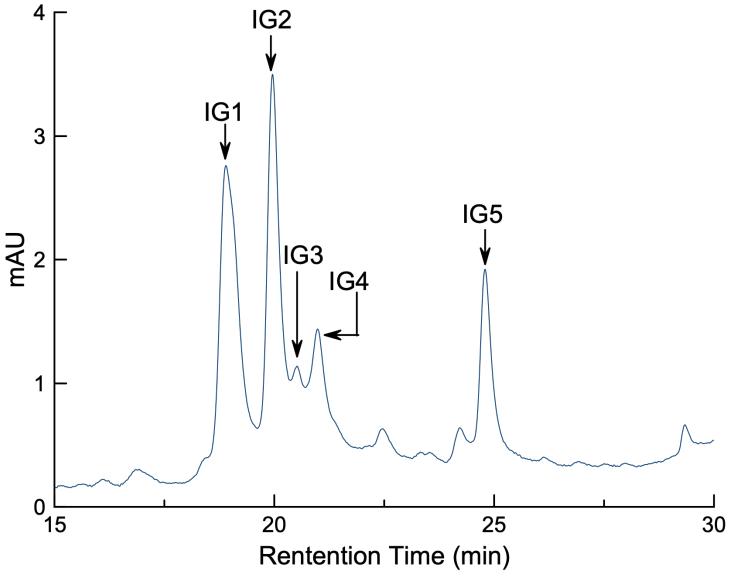


***Figure 11.*** *Chromatogram of the Isorhamnetin Glycosides (IGs) (IG1-IG5) identified in Opuntia ficus-indica (OFI) flour from HPLC-UV at 365 nm.*

***Table 4.*** *Isorhamnetin Glycosides Identification in HPLC-UV.*

| Peak ID | Retention time (min) | Compound | UV λ max |
|---|---|---|---|
| IG1 | 18.907 | Isorhamnetin glucosyl rhamnosyl rhamnoside | 254, 354 |
| IG2 | 19.962 | Isorhamnetin glucosyl rhamnosyl pentoside | 253, 354 |
| IG3 | 20.512 | Isorhamnetin glucosyl rhamnosyl methylpentoside | 253, 354 |
| IG4 | 20.985 | Isorhamnetin glucosyl pentoside | 253, 354 |
| IG5 | 24.798 | Isorhamnetin glucosyl rhamnoside | 253, 354 |

On the other hand, it was noticed that isorhamnetin glycosides concentration was percentage dependent in the PLA and PCL nanofibers loaded with 10%, 30%, 50% and 70% w/w of OFI flour (**Figure 12**). Specifically, PLA nanofibers showed a concentration range of isorhamnetin glycosides between 235.79 ± 18.09 and 904.33 ± 58.75 µg IsoEq/g fiber, while PCL fibers showed a concentration range between 126.16 ± 34.82 to 3177.82 µg IsoEq/g fiber. Therefore, the nanofibers that showed the highest isorhamnetin glycoside concentration were the ones with 70% w/w of OFI flour, which allowed to load 3177.82 ± 789.77 µg IsoEq/g of fiber and 904.33 ± 58.75 µg IsoEq/g of fiber in PCL and PLA fiber, respectively.

In other words, the general concentration of isorhamnetin glycosides in the PLA fibers was higher than these compound's concentration in PCL fibers incorporating 53.51%, 63.74%, 74.92% more isorhamnetin glycosides than PCL fiber when was added10%, 30%, and 50% (w/w) of OFI flour, respectively. However, with 70% of OFI flour, the PCL nanofiber allowed to load 3 times more isorhamnetin glycosides in comparison to the PLA nanofiber loaded with 70% w/w of OFI flour.

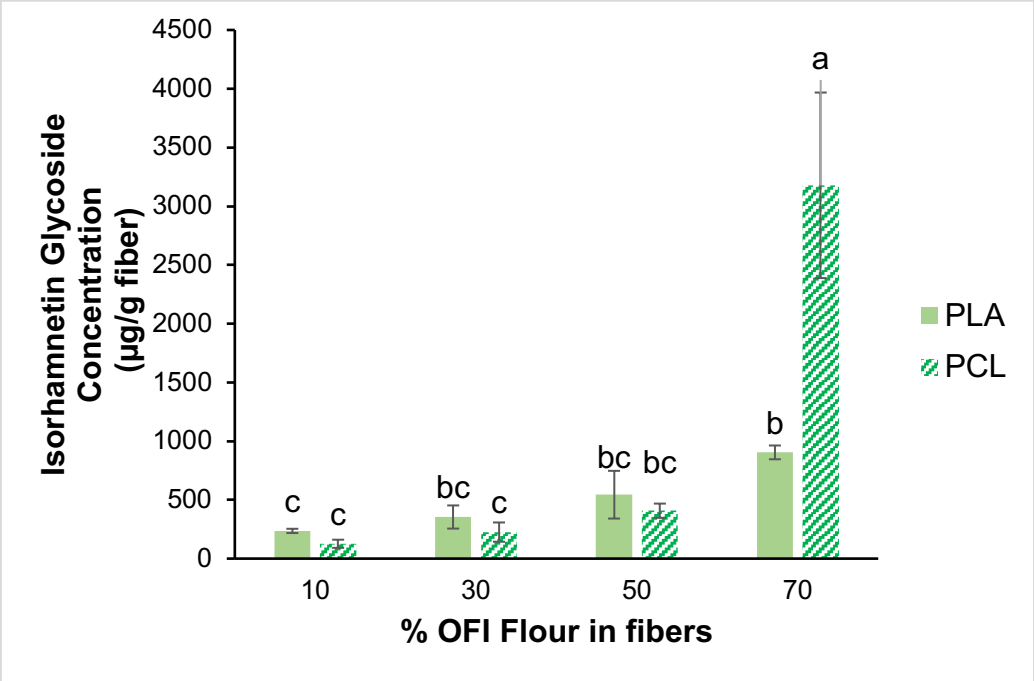


***Figure 12.*** *Isorhamnetin glycoside concentration in Polylactic acid (PLA) and Polycaprolactone (PCL) electrospun nanofibers with 10%, 30%, 50% and 70% w/w of Opuntia ficus-indica (OFI) flour.* [a,b,c] *Means with different letter are significantly different p<0.05 by Tukey's Test.*

Although the highest concentration of all fibers was observed in PCL nanofibers with 70% w/w OFI flour, which was statistically different to the other treatments, in general, it was observed that in all the other percentages of OFI flour (10-50%), the PLA fibers showed the highest concentration range in comparison to PCL nanofibers. Structural characteristics responsible for this behavior will be further discussed (*section 3.4*). The nanofibers with 70% w/w of OFI flour of both polymers were selected to continue with the next assays.

## 3.4 Nanofiber Mesh Chemical Characterization by FTIR

The molecular interactions between functional groups during the incorporation of isorhamnetin glycosides to the PLA and PCL nanofibers are shown in the FTIR spectra. Specifically, the OFI flour spectra shows a broad peak at 3311 $cm^{-1}$ attributed to O-H stretching due to the alcohols in its structure, in addition two medium peaks appeared at 2919-2850 $cm^{-1}$ corresponding to C-H stretching from alkene compounds. In 1603 $cm^{-1}$ a medium peak corresponding to C=C stretching appeared corresponding to a conjugated alkene, and a set of peaks in 1370 and 1315 $cm^{-1}$ was shown corresponding to O-H blending attributed to the phenol compounds, and lastly, a strong peak in 1032 was observed due to the C-O stretching of the structure (**Table 5, Figure 13**), a similar pattern of peaks where reported in literature (Catanzano et al., 2021; Gheribi et al., 2018; Otálora et al., 2019).

***Table 5.*** *FTIR peak identification of Opuntia ficus-indica flour.*

| Wavenumber ($cm^{-1}$) | Appearance | Group | Compound Class | Reference |
|---|---|---|---|---|
| 3311 | strong, broad | O-H stretching | Alcohol | Gheribi, et al., 2018; Catanzano et al., 2021; Otálora et al., 2019 |
| 2919, 2850 | medium | C-H stretching | Alkane | |
| 1603 | medium | C=C stretching | Conjugated alkene | |
| 1370, 1315 | medium | O-H bending | Phenol | |
| 1032 | strong | C-O stretching | | |

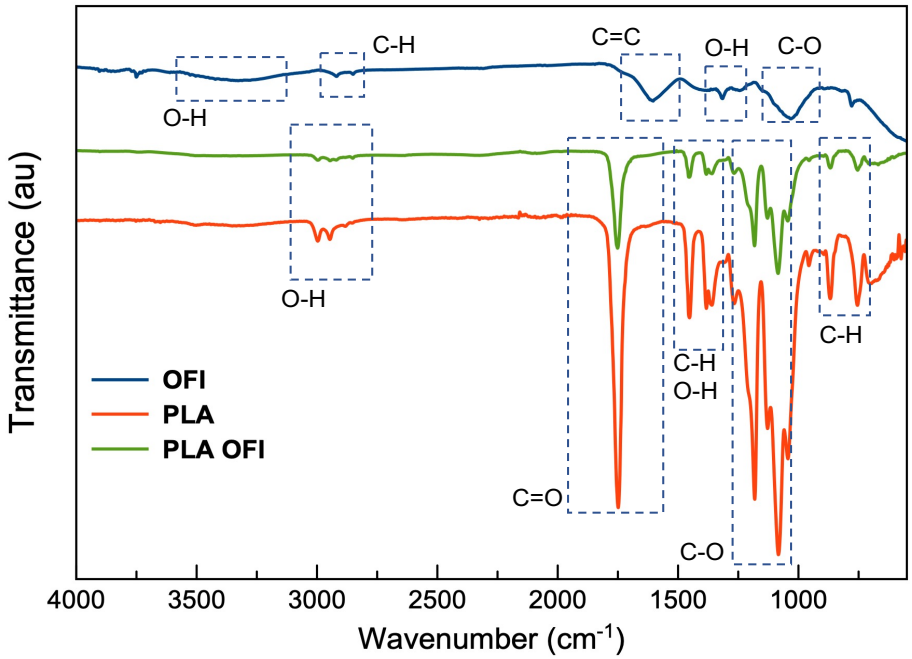


***Figure 13.*** *FTIR spectra of electrospun Polylactic acid (PLA) and PLA OFI nanofibers and Opuntia ficus-indica (OFI) flour.*

On the other hand, PLA control nanofiber showed its distinctive peaks between 2996-755 $cm^{-1}$ (**Table 6, Figure 13**). Specifically, in 2996 and 2946 $cm^{-1}$ showed a weak peak corresponding to the O-H stretching from the carboxylic acid group. Additionally, in 1748 $cm^{-1}$ a strong peak was shown due to C=O stretching, also corresponding to the carboxylic acid group. It was also observed a medium peak at 1452 $cm^{-1}$ corresponding to the C-H bending of the methyl group, and at 1382 and 1360 $cm^{-1}$ it was observed two medium peaks corresponding to O-H bending. The peaks shown in 1181, 1107, 1083, 1043 $cm^{-1}$ correspond to C-O stretching from secondary alcohols, and finally in 867 and 755 $cm^{-1}$ it was observed the peaks corresponding C-H bending. Similar peak pattern was described in previous research (K. Choi et al., 2013; García et al., 2012; Paragkumar N et al., 2006).

***Table 6**. FTIR peak identification of electrospun Polylactic acid (PLA) nanofibers with and without Opuntia ficus-indica (OFI) flour.*

| Wavenumber ($cm^{-1}$) | Appearance | Group | Compound Class | Reference |
|---|---|---|---|---|
| 2996, 2946 | weak | O-H stretching | Carboxylic acid | Choi et al., 2013; García et al., 2012; Paragkumar N et al., 2006 |
| 1748 | strong | C=O stretching | Carboxylic acid | |
| 1452 | medium | C-H bending | Alkane, methyl group | |
| 1382, 1360 | medium | O-H bending | Alcohol | |
| 1181 | strong | C-O stretching | | |
| 1107, 1083, 1043 | strong | C-O stretching | Secondary alcohol | |
| 867 | medium | C-H bending | | |
| 755 | medium | C-H bending | | |

It was observed that when adding OFI flour to the PLA electrospun nanofibers OFI flour peaks disappear, and PLA peaks lower its intensity. These had previously been reported by Gheberi, et al., 2018, and it is related to the involvement of the corresponding functional groups in some reactions. Specifically, in the PLA nanofibers loaded with OFI Flour, the peak in 2996 $cm^{-1}$ and 2946 $cm^{-1}$ is now attributed to OH intermolecular bonding, i.e., hydrogen bonding, between glycosides and PLA, as a result of the OH groups provided by PLA, and the bands showed at 1043 $cm^{-1}$ was related to the polysaccharide back bone, along with the band in 867 $cm^{-1}$, related to the sugars in the glycosides (**Figure 14**) (Gheribi et al., 2018; Otálora et al., 2019). Given this information, it could be considered that due to the availability of several OH and C=O groups in the PLA structure, it is easier to bond with the isorhamnetin glycosides, which is why in section 3.3 it was shown a higher concentration range in the PLA nanofibers loaded with 10%, 30% and 50% w/w of OFI flour, in comparison to the PCL nanofibers.

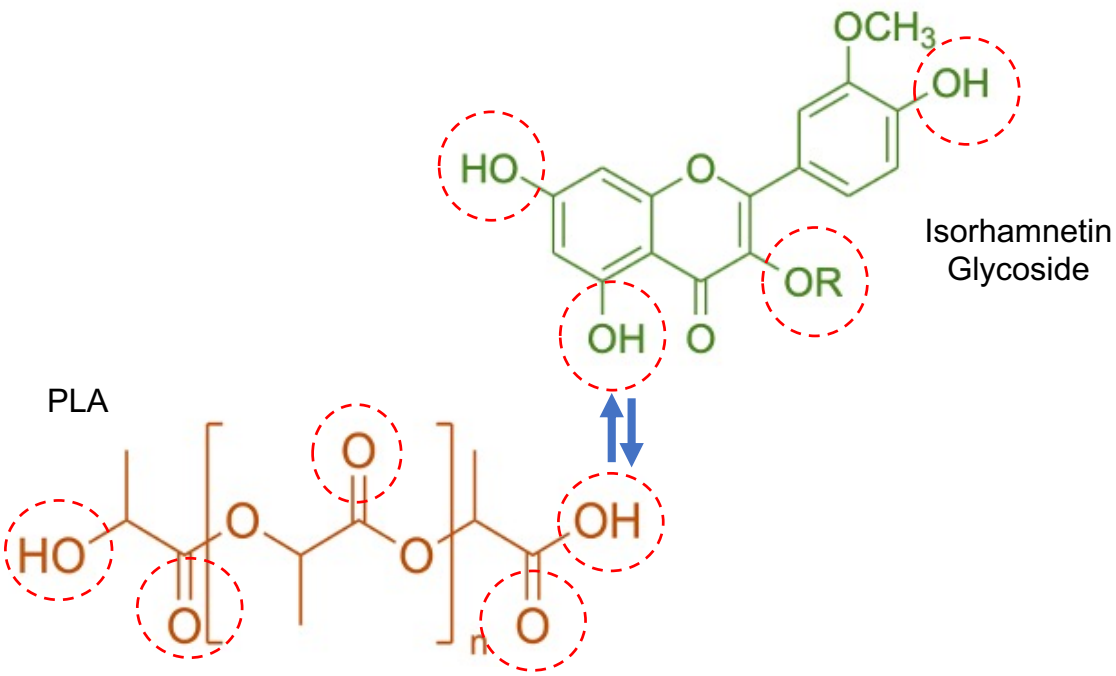


***Figure 14**. Hypothetical chemical interactions among polylactic acid (PLA) and isorhamnetin glycosides (IGs) during the formation of nanofibers. Circled in red are the groups where the possible interactions can be given. R corresponds to the sugar moiety present in IGs.*

On the other hand, FTIR spectra of the electrospun PCL nanofibers with and without OFI flour (**Table 7, Figure 15**) shows its characteristic peaks in a range between 2945 and 732 $cm^{-1}$. Specifically, two peaks were shown in 2495 and 2866, corresponding to O-H stretching due to the carboxylic acid group, additionally, a strong peak in 1722 $cm^{-1}$ was observed corresponding to the C=O vibration from the ketone. It was also shown a peak in 1365 $cm^{-1}$ corresponding to O-H bending from the alcohol in the structure. Furthermore, in the range between 1294 to 1047 $cm^{-1}$, several peaks were shown corresponding to C-O stretching, and in 732 $cm^{-1}$ corresponding to C-H bending. A similar pattern has been previously described by some authors(Behere et al., 2020; Mohandesnezhad et al., 2020).

Similar to the previously described with PLA OFI nanofibers, when loading the PCL nanofibers with OFI flour, the relevant peaks of OFI flour disappear, and the PCL relevant peaks slightly decrease its intensity. Given this information, it is believed that the peaks shown in 2945 and 2866 $cm^{-1}$ correspond to the hydrogen bonds formed between PCL and the isorhamnetin glycosides, or the peak in 1238-

1294 $cm^{-1}$ correspond to C-O bonding between PCL and isorhamnetin glycosides (**Figure 16**) (Mehteroğlu et al., 2020).

In this specific case, the fact that the isorhamnetin glycosides concentration in the PCL fibers loaded with 70% w/w of OFI flour was 3 times higher could be explain by the fact that, given that the OH groups with which is easier to bond are in the ends of the chain, a better, more compact, stacking could be reached by Van der Waals interaction, which could allow better interaction between the PCL and isorhamnetin glycoside.

***Table 7**. FTIR peak identification of electrospun polycaprolactone (PCL) nanofibers with and without Opuntia ficus-Indica (OFI) flour.*

| Wavenumber ($cm^{-1}$) | Bond | Vibration Mode | Compound | Reference |
|---|---|---|---|---|
| 2945, 2866 | strong, broad | O-H stretching | Carboxylic acid | Mehteroğlu et al., 2020 |
| 1722 | strong | C=O | Aliphatic ketone | |
| 1365 | medium | O-H bending | Acohol | |
| 1294 | medium | C-O stretching | | |
| 1238 | medium | C-O stretching | | |
| 1165, 1108, 1047 | strong | C-O stretching | Alcohol | |
| 732 | medium | C-H bending | | |

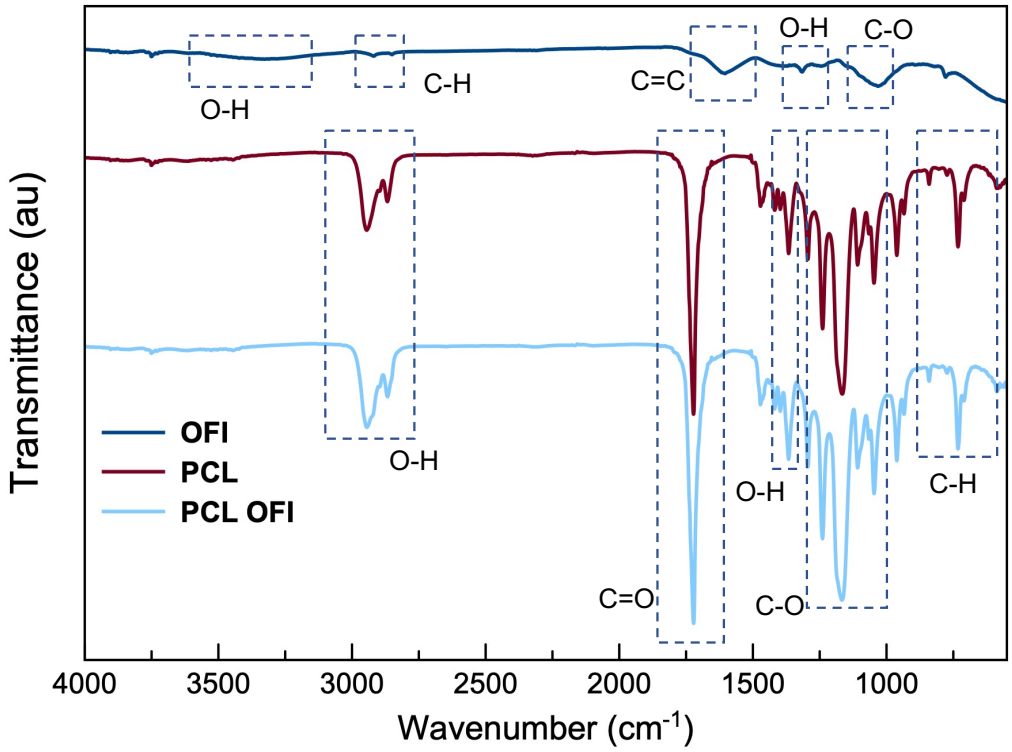


***Figure 15.*** *FTIR spectra of electrospun polycaprolactone (PCL), PCL OFI (Opuntia ficus-indica) nanofibers and OFI flour.*

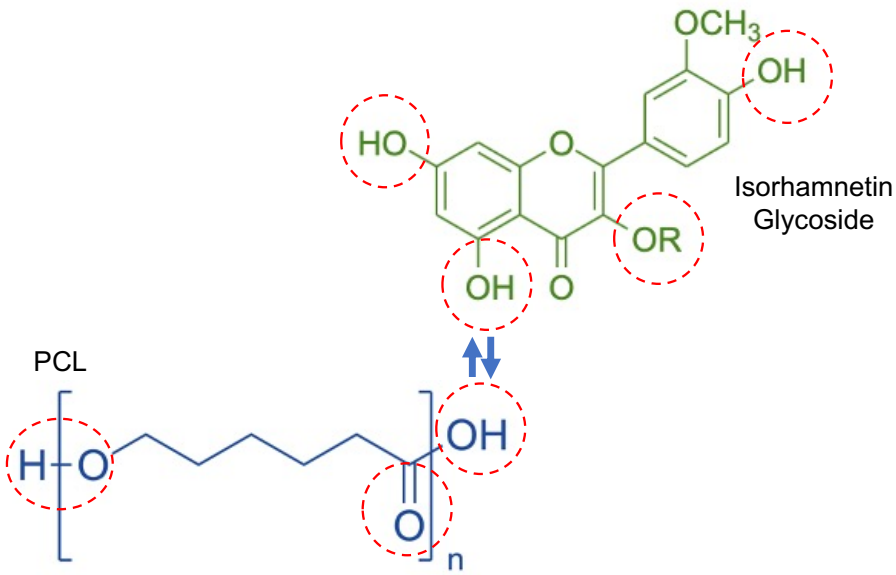


***Figure 16****. Hypothetical chemical interactions among polycaprolactone (PCL) and isorhamnetin glycosides (IGs) during the formation of nanofibers. Circled in red are the groups where the possible interactions can be given. R corresponds to the sugar moiety present in IGs.*

## 3.5 Nanofiber Mesh Morphological Characterization by SEM

SEM morphological characterization showed that all the fibers are randomly oriented (**Figure 17, 18**). PLA nanofibers presented a porous surface while PCL nanofibers presented a bead-like structure. Several researchers observed that high voltages are responsible for the incidence of beads (Behere et al., 2020; Zhao et al., 2008). It was stated that when the electric field strength was below 1.25 kV/cm beads appear concurrently in nanofibers, contrary to when the electric field strength is above 1.5 kV/cm. Other factors that affect morphology and diameter of electrospun nanofibers are type of polymer, concentration, polarity, feeding rate of polymer solution and strength of the applied electric field, which is defined as the voltage rate over the distance between the spinneret and the collector (Zhao et al., 2008).

On the other hand, it was reported that cell growth behavior was dependent on the fiber orientation, in other words, the more aligned, the better cell proliferation and elevated alkaline phosphatase (ALP) activity (Guo et al., 2015).

In comparison, it was observed that PLA fibers showed better alignment than PCL fibers. On the other hand, it was observed a decrease of beads with the addition of OFI flour to the PLA nanofibers. Furthermore, with the addition of OFI flour to the PCL nanofibers, an increment in the thickness of the fibers was observed.

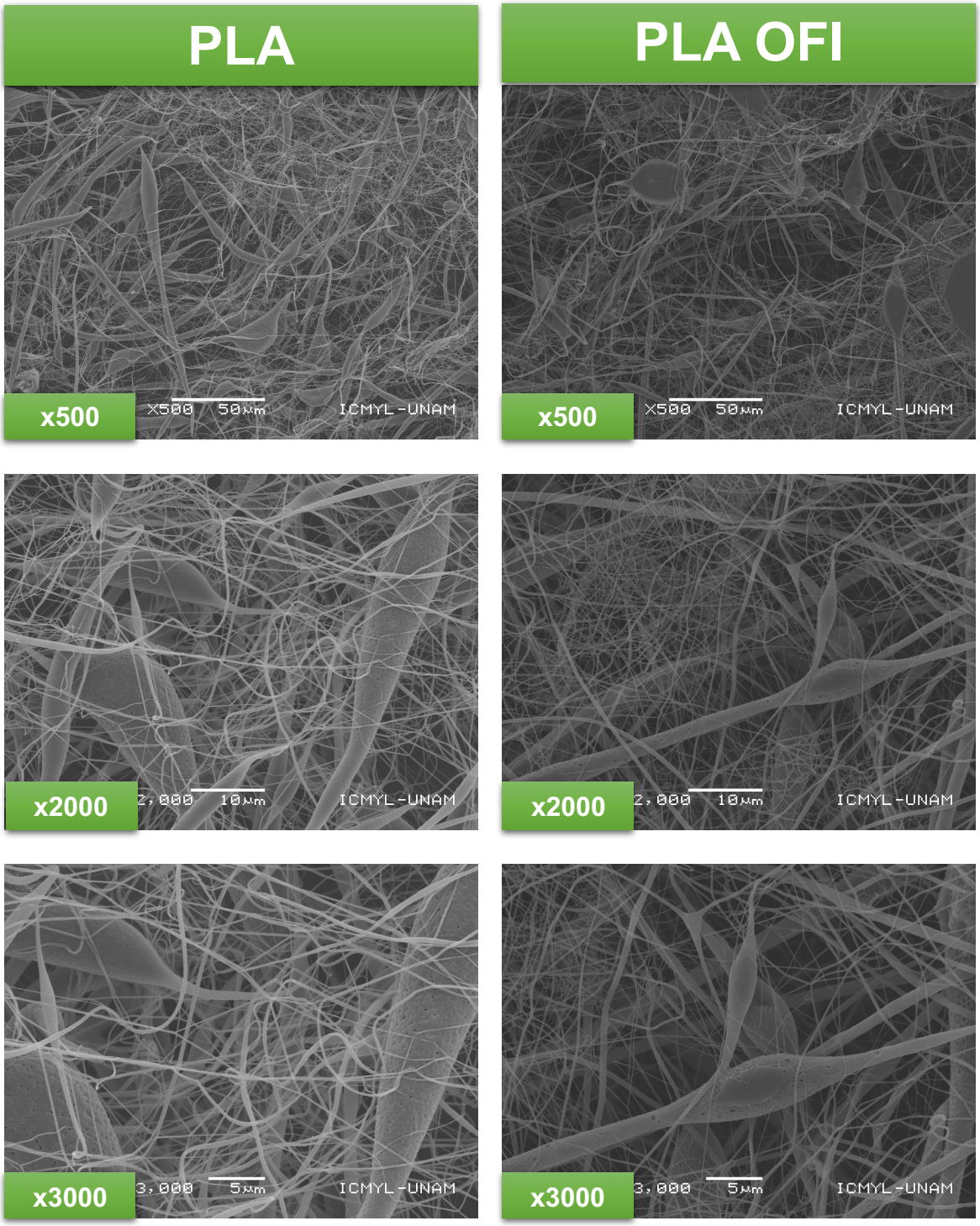


***Figure 17.*** *SEM images of the polylactic acid (PLA) and PLA OFI (Opuntia ficus-indica) electrospun nanofiber meshes at different amplifications.*

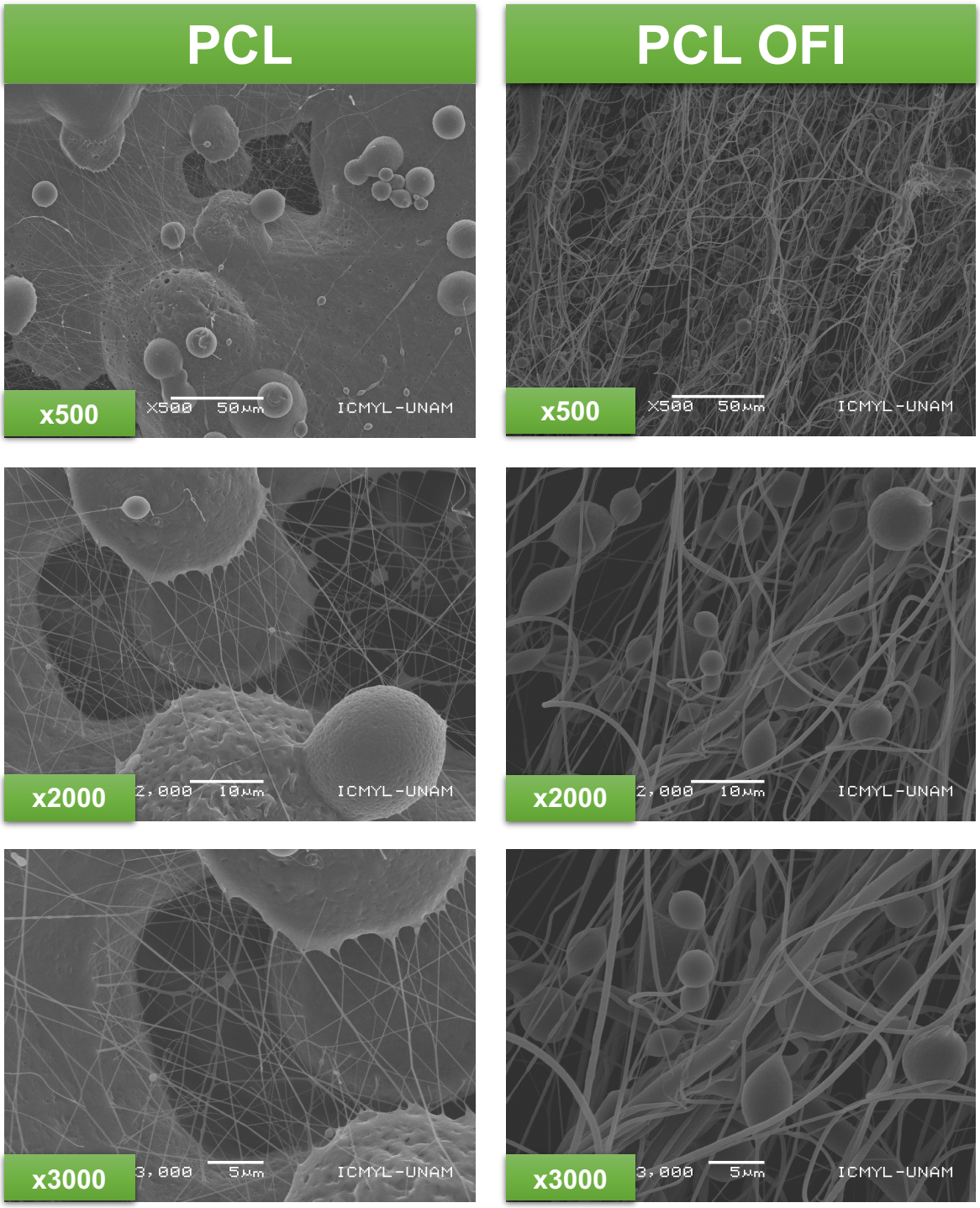


***Figure 18.*** *SEM images of the polycaprolactone (PCL) and PCL OFI (Opuntia ficus-indica) electrospun nanofiber meshes at different amplifications.*

## 3.6 Release Analysis of Isorhamnetin Glycosides

A release of total isorhamnetin glycosides by 14.9 ± 2.5% (134.75 µg IsoEq/g fiber) and 8.5 ± 3.3% (270.11 µg IsoEq/g fiber) was observed in PLA and PCL nanofibers respectively, after 48h with no significant difference, in comparison to its initial concentration (**Figure 19**). In comparison, some authors have reported a total release of quercetin of 22% from the amaranth protein isolate-pullulan nanofibers, which even it's a different polymeric matrix, it can give an approach to the release pattern that flavonoids follow in nanofibers (Aceituno-Medina et al., 2015). These release patterns depend on the chemical and morphological characteristics of the fiber, and also in other properties like pH, where at pH 7 the release behavior is higher (Khoshnoudi-Nia et al., 2020).

Particularly, the higher release rate in PLA electrospun nanofiber with 70% of OFI flour, could be due to its interaction, as seen in section 3.5, since it has more molecular groups where the attachment to the isorhamnetin glycosides (IGs) could be done via a hydrogen bond, however, its staking would be less compact than that of the PCL-IGs, since PCL only has two possible attachment groups with the IGs and could have a more compact stacking, which would allow IGs to release easier from PLA than from PCL.

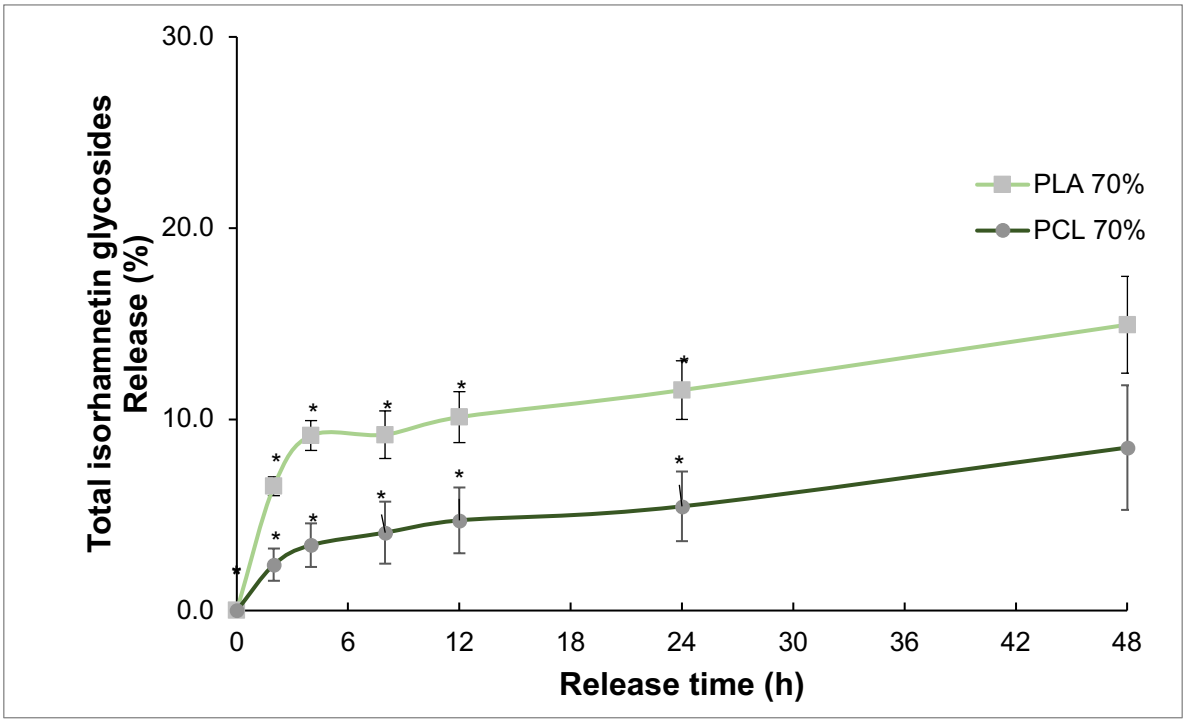


***Figure 19.*** *Total Isorhamnetin Glycosides Release (%) in polycaprolactone (PCL) and polylactic acid (PLA) electrospun nanofibers with 70% w/w (Opuntia ficus-indica) OFI-Flour in a 48h period.* * *Means with asterix are significantly different p<0.05 by Tukey's test.*

On the other hand, the release pattern of each individual glycoside in each fiber was observed (**Figure 20, 21**). The highest release percentage was observed in IG3 for both fibers, specifically, in PLA nanofiber it was observed a maximum release of 21.6 ± 1.64%, while in PCL nanofiber, it was observed a maximum release of 10.0 ± 1.35%. These results could be attributed to the structure of the IG3, specifically to the nature of the sugar moiety. It has been reported that L-rhamnose is a monosaccharide with great ease of hydrolysis, which is related to the ease of breaking bonds, and also, the position of substitution is important (Harborne, 1965).

On the other hand, it could also be attributed this effect to the fact that the glycosides with the highest release percentage (IG2, IG3, IG5) on both fibers, are the most abundant glycosides found in OFI flour (Antunes-Ricardo et al., 2014a).

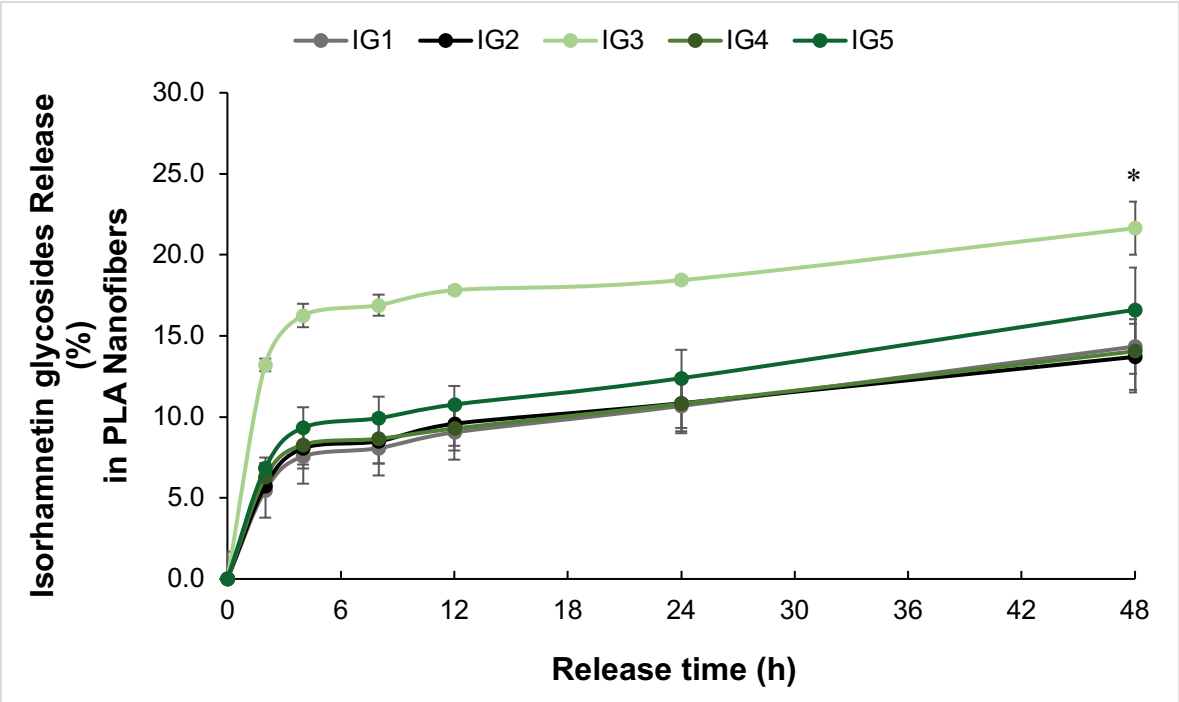


***Figure 20.*** *Isorhamnetin Glycosides Release (%) in polylactic acid (PLA) electrospun nanofibers with 70% w/w (Opuntia ficus-indica) OFI flour in a 48h period.* * *Means with asterix are significantly different p<0.05 by Tukey's test.*

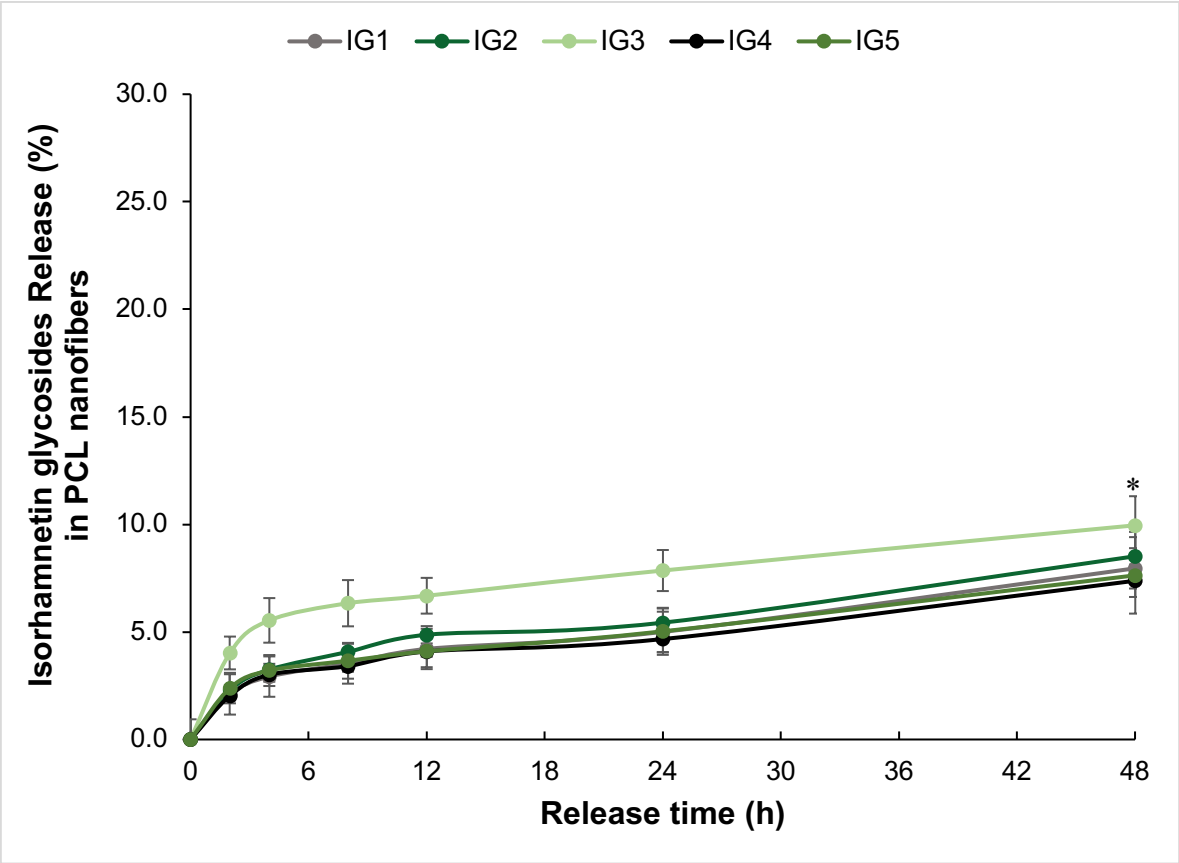


***Figure 21.*** *Isorhamnetin Glycosides Release (%) in polycaprolactone (PCL) electrospun nanofibers with 70% w/w (Opuntia ficus-indica) OFI-Flour in a 48h period.* * *Means with asterix are significantly different p<0.05 by Tukey's test.*

## 3.7 Biodegradation Rate Assay

Biodegradation rate assay in PLA and PCL fibers with and without OFI flour was carried (**Figure 22**) and it was observed a biodegradation rate between 26.83% and 5.52% after 24h, and between 63.81% and 5.15% after 48h. The highest biodegradation rate was observed in the PLA control fibers (63.81%) after 48h, followed by PLA control fibers after 24h (26.83%). In the PCL fibers the highest degradation rate was observed in the PCL control fiber after 24h (18.08%). On the other hand, the nanofibers loaded with isorhamnetin glycosides were the ones with the lower biodegradation rate, where it was observed a higher degradation rate after 24h rather than in 48h.

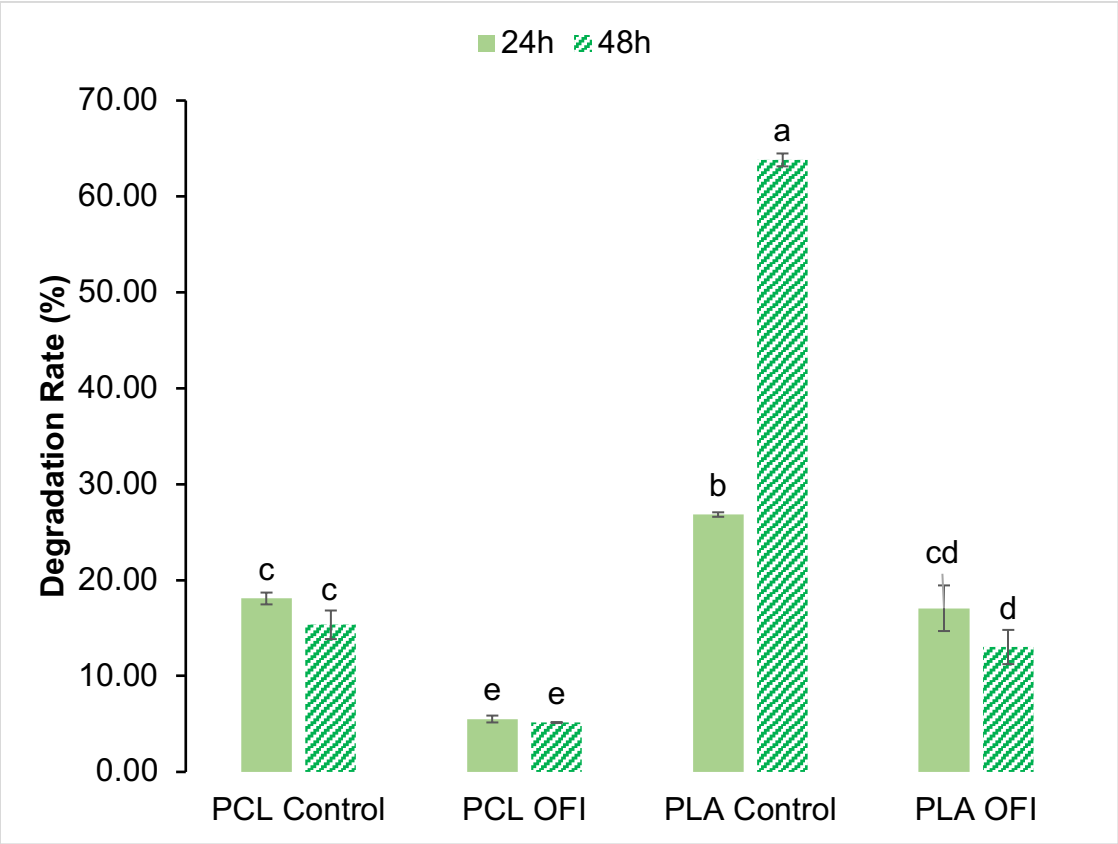


***Figure 22.*** *Degradation rate in 24h and 48h of polycaprolactone (PCL) and polylactic acid (PLA) electrospun nanofibers with and without 70% w/w (Opuntia ficus-indica) OFI flour.* [a,b,c,d,e] *Means with different letter are significantly different p<0.05 by Tukey's test.*

It has been proven that the combination of natural and synthetic polymers can improve nanoparticle properties. Studies in electrospun nanofibers have shown that the addition of a natural extract, like curcumin, improves durability in degradation media, which makes an ideal scaffold for the application as patches (Khoshnoudi-Nia et al., 2020). On the other hand, the biodegradability of PLA at a slow rate has been reported and it was observed that PCL degrades at a much slower rate than PLA (Herrero-Herrero et al., 2018). In addition, it is known that the proteinase K cleaves bonds adjacent to the carboxylic groups (Hosseini-Koupaei et al., 2016), and since PLA has more carboxylic groups, it can be explained why it has higher degradability rate in comparison to PCL electrospun nanofiber, and also why with the addition of OFI flour, it disminishes in comparison to the control fibers, since in control fibers there are more free carboxylic groups, while in OFI flour nanofibers it is bound with these carboxylic groups.

## 3.8 Swelling Rate Assay

Swelling rate (**Figure 23**) was observed between 89.99% and 64.07% after 24h in the PLA and PCL nanofibers, with and without OFI flour. Specifically, the fibers loaded with isorhamnetin glycosides showed the highest swelling ratio, where PLA OFI had 89.99% and PCL OFI had 81.38%. On the other hand, control fibers of both PLA and PCL polymers, showed the lowest swelling ratio, with 64.07% and 68.15% respectively. There was no significative difference between control and OFI treatments ($p<0.05$).

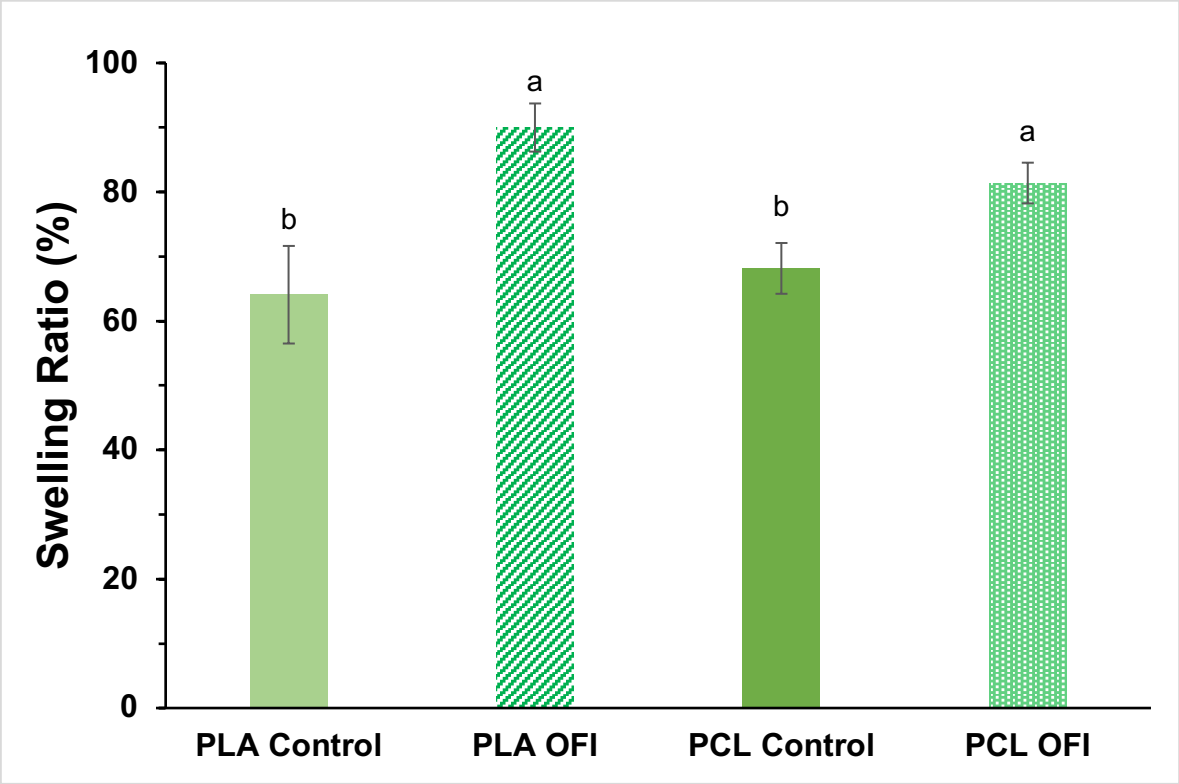


***Figure 23**. Swelling Ratio (%) of polylactic acid (PLA) and polycaprolactone (PCL) electrospun nanofibers with and without Opuntia ficus-Indica flour after 24h.*
*[a,b]Means with different letter are significantly different p<0.05 by Tukey's test.*

Swelling ratio is reported to be affected by several parameters such as preparation method of the material, mat thickness, polymer molecular structure, specifically its hydrophilic and hydrophobic properties, polymer molecular weight, macropores and polymer stacking density. On the other hand, authors have reported that the addition of glycosides and other natural extracts to the structure of materials enhances swelling and water absorption capacity (Khoshnoudi-Nia et al., 2020;

Mehteroğlu et al., 2020). Specifically, by the addition of OFI flour to the electrospun nanofibers, more OH groups are available for the formation of hydrogen bonds with the isorhamnetin glycosides, so it presents higher swelling and water absorption capacity.

## 3.9 Isorhamnetin glycosides cytotoxicity in hFOB cells

The cytotoxicity of isorhamnetin glycosides in both PLA and PCL nanofibers, with and without OFI flour, were tested *in vitro* using the hFOB cells (**Figure 24, 25**).

Specifically, it was observed in the PLA nanofiber (**Figure 24**) a viability of 87% in control fiber, and of 86.38% in fiber with OFI flour after 24h. In addition, after 48h it was observed a viability of 86.62% in control fiber, and 80.27% in fiber with OFI flour. There wasn't a significant effect in the cell viability in the fibers during 24h or 48h, so it can be considered that there isn't a significant added effect on cell viability due to the isorhamnetin glycosides.

On the other hand, when adding OFI flour to the PCL fibers (**Figure 25**) a viability of 85.25% in control fiber, and of 93.50% in fiber with OFI flour after 24h. In addition, after 48h it was observed a viability of 75.24% in control fiber, and 66.89% in fiber with OFI flour. In 24h there was a positive effect from the IGs in the hFOB cell viability, however at 48h a cytotoxic effect starts showing.

Previous work has reported the cytotoxic effect of the isorhamnetin glycosides, which has been attributed to the fact that, in addition to flavonoids, there might be other phytochemicals that could contribute to the induction of cell death; and it was also reported that this effect is affected on the glycosylation pattern, due to the change in their physicochemical properties that influences how they incorporate into cells, or the cell mechanisms that they can induce (Antunes-Ricardo et al., 2014b). This last observation is linked to the results obtained in section 3.3, **Figure 12**, where it can be observed that PCL nanofibers loaded with 70% of OFI flour has higher IGs content than the PLA nanofibers also loaded with 70% of OFI flour.

Furthermore, cell layout in both PLA and PCL nanofibers can be observed by the Hoesch tinction. As observed (**Figure 26**) in PLA OFI nanofiber, cells appeared to be more pilled up and had a better alignment than in PCL OFI nanofibers. In

addition, in PLA OFI nanofiber, cells seem to be agglomerated in some zones, but it shows a more homogeneus distribution among the fiber than in PCL OFI nanofiber. On the other hand, in PCL OFI nanofiber there's a more heterogeneous distribution among the fiber, however there's more distance between cells in comparison to the PLA OFI nanofibers. In order to better mimic hFOB ECM it is preferred to have less distance between the cells, so there's a more dense cell layer, reducing brittleness of the tissue. This can also confirm that there is better cell arrangement in the PLA OFI nanofiber, in comparison to PCL OFI nanofiber (Ramírez-Fernández et al., 2013).

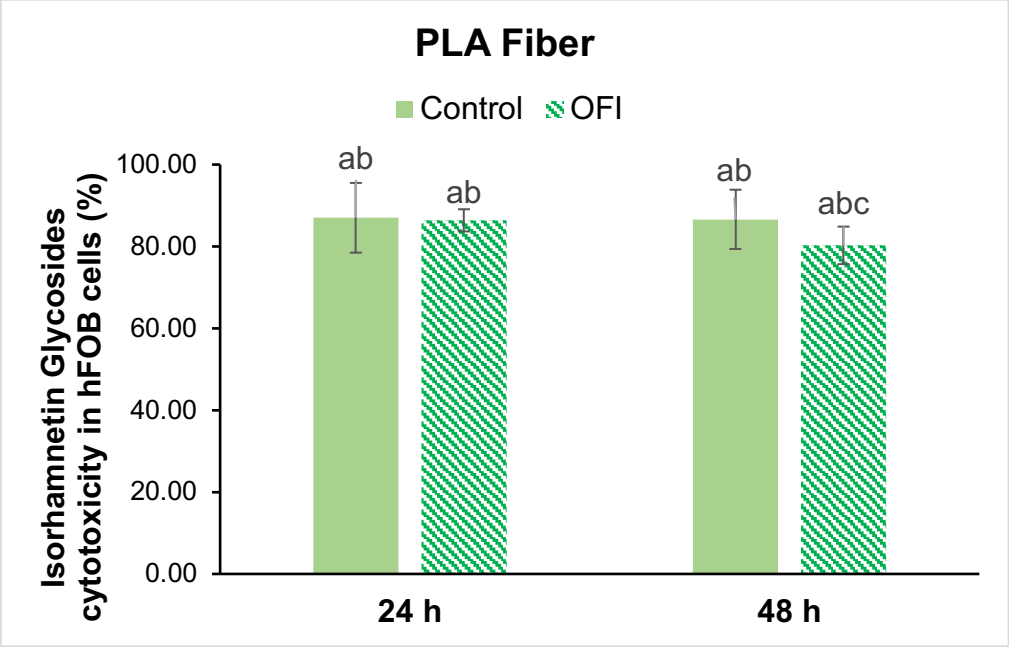


***Figure 24.*** *Isorhamnetin Glycosides cytotoxicity in hFOB cells (%) of polylactic acid (PLA) electrospun nanofibers with and without Opuntia ficus-indica (OFI) flour in 24h and 48h,* [a,b,c] *Means with different letter are significantly different p<0.05 by Tukey's test.*

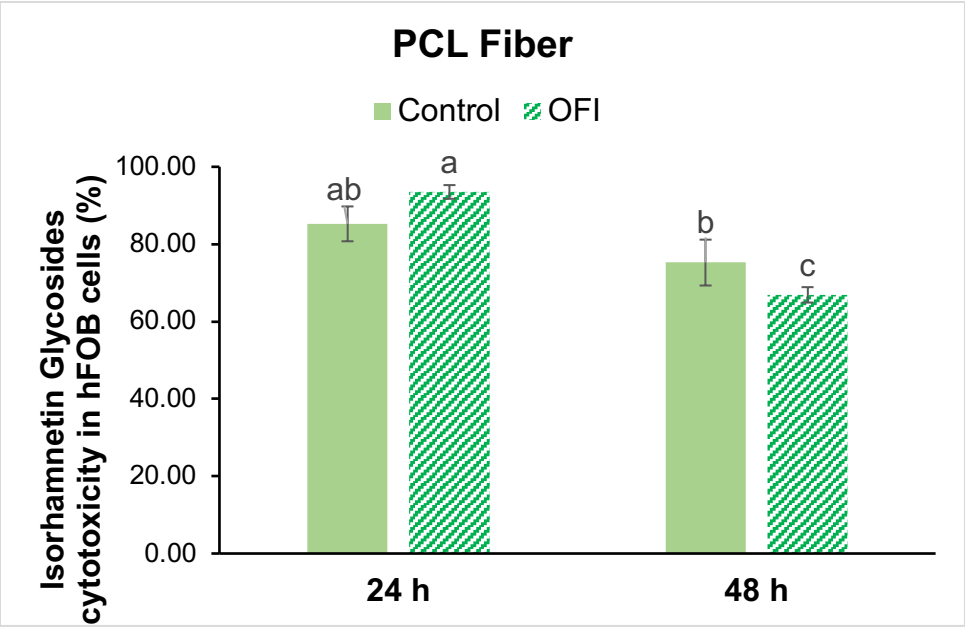


***Figure 25.*** *Isorhamnetin Glycosides cytotoxicity in hFOB cells (%) of polycaprolactone (PCL) electrospun nanofibers with and without Opuntia ficus-indica (OFI) flour in 24h and 48h. , [a,b,c] Means with different letter are significantly different p<0.05 by Tukey's test.*

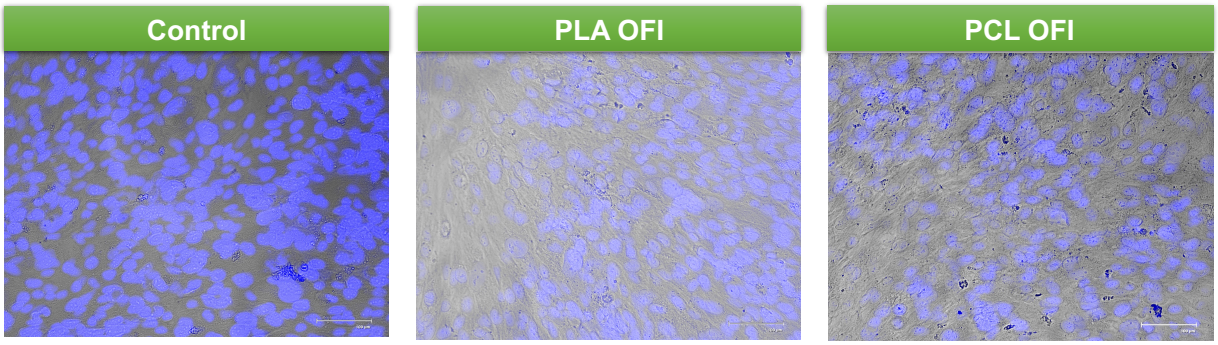


***Figure 26.*** *hFOB cell layout by Hoesch Tinction in polylactic acid (PLA) and polycaprolactone (PCL) electrospun nanofibers with Opuntia ficus-indica (OFI) flour.*

## 3.10 Cell Differentiation

Cell differentiation was observed after 7 days (**Figure 27**). It was noticed that in day one of cell differentiation, in all fibers and in the control, the cells were expanded. In addition, cells in control, PLA and PLA OFI fibers appear to be closer together than in PCL and PCL OFI fibers. On the other hand, in PLA and PLA OFI nanofibers, it was observed that the cells were more expanded, bigger, and the cells in PLA OFI showed more alignment and a more compact morphology, in comparison to the control. Moreover, in PCL and PCL OFI nanofibers it was observed that there

were more cells expanded since day 1, specifically in the PCL nanofiber there's more agglomeration than in PCL OFI nanofiber. In both PCL and PCL OFI after 7 days, it can be observed that there are several arrangements, directions and cell sizes, according to the zone of the fiber. In addition, in PCL nanofiber it can be observed some expanded cells. Furthermore, in PCL OFI nanofiber it can be observed that some cells are pilled.

After 7 days, it was observed that all cells showed maturation. Particularly, it can be observed that the fibers with OFI flour less visible cells in comparison to the fibers without OFI flour. Specifically, it can be observed a better cell morphology in PLA OFI nanofiber, which can be related to the previously discussed in section 3.5, that fiber alignment enhances cell growth and proliferation.

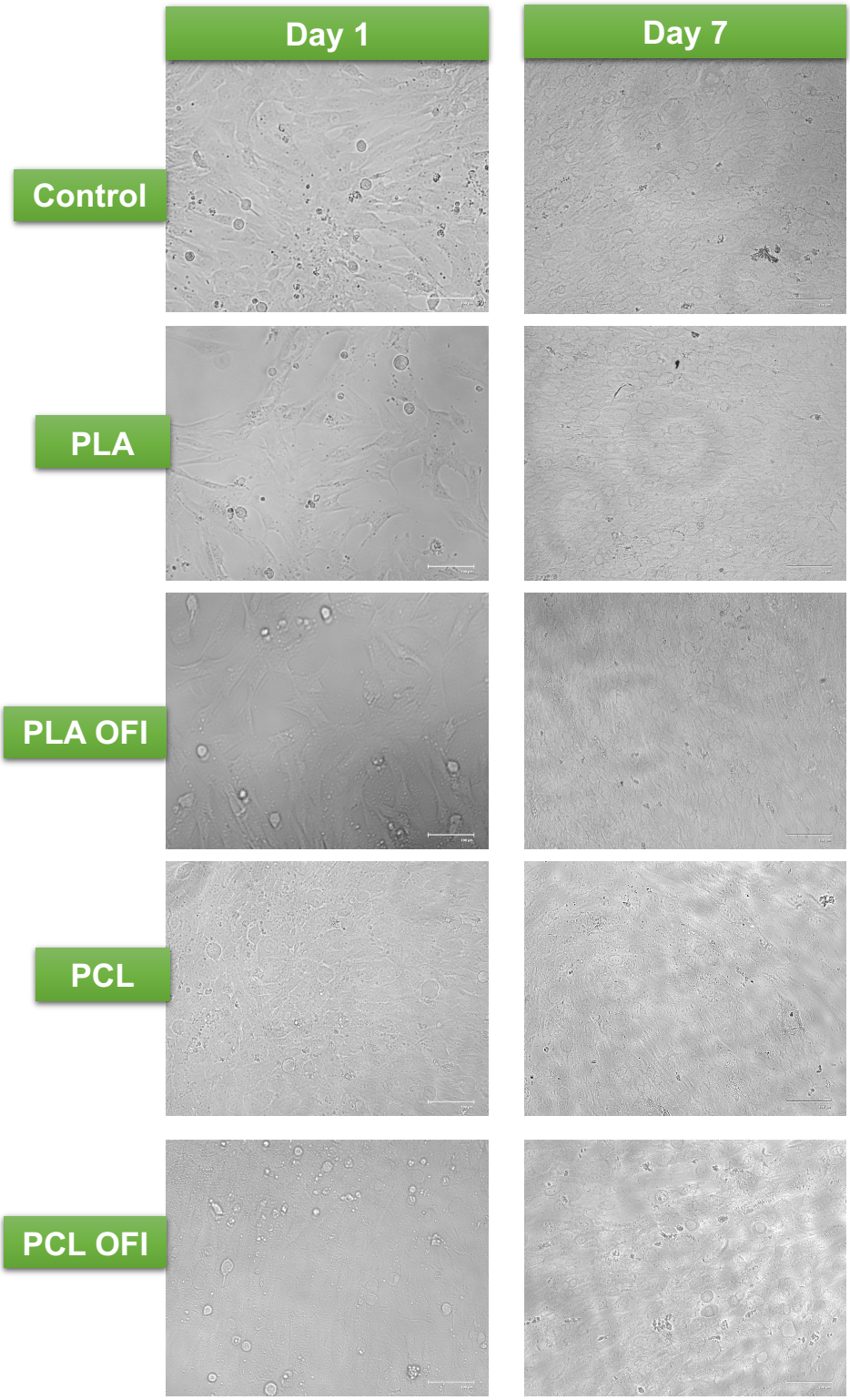


***Figure 27**. hFOB cell differentiation after 7 days in polylactic acid (PLA) and polycaprolactone (PCL) electrospun nanofibers with and without Opuntia ficus-indica (OFI) flour.*

## 3.11 hFOB maturation

Measurement of alkaline phosphatase (ALP) activity of hFOB cells (**Figure 28**) was used as a marker for osteoblastogenesis. It was observed that PLA nanofiber loaded with OFI flour showed higher maturation in comparison to PLA control fiber. On the other hand, PCL control nanofiber showed higher hFOB maturation, however it showed no significant difference with the PCL OFI nanofiber.

A positive effect of the isorhamnetin glycosides in the PLA nanofiber was observed, since it increased 0.008 the absorbance value. However, on the PCL OFI nanofibers there is no significant effect from the isorhamnetin glycosides.

As previously described, cell growth behavior is dependent on the fiber orientation, in other words, the more aligned, the better cell proliferation and elevated alkaline phosphatase (ALP) activity (Guo et al., 2015), and as mentioned before, PLA showed better alignment in its morphology.

It is known that the alkaline phosphatase level is an indicator of successful osteoblast differentiation, which plays a crucial in the mineralization of bone. Given this information, we could assume that there is evidence of maturation and potential mineralization by the IGs in PLA nanofibers, which could enhance bone formation (Karadeniz et al., 2014). ALP appears to act both to increase the local concentration of inorganic phosphate, a mineralization promoter, and to decrease the concentration of extracellular pyrophosphate, an inhibitor of mineral formation (Golub & Boesze-Battaglia, 2007). These results are of relevant because mineralization is one of the main steps in bone remodeling, which consists of the resorption of a certain amount of bone by osteoclasts, likewise the formation of osteoid matrix by osteoblasts, and its subsequent mineralization. Once the matrix is mineralized, some osteoblasts remain trapped within, becoming transformed into osteocytes, which will then initiate bone formation or resorption (Hernández-Gil et al., 2006).

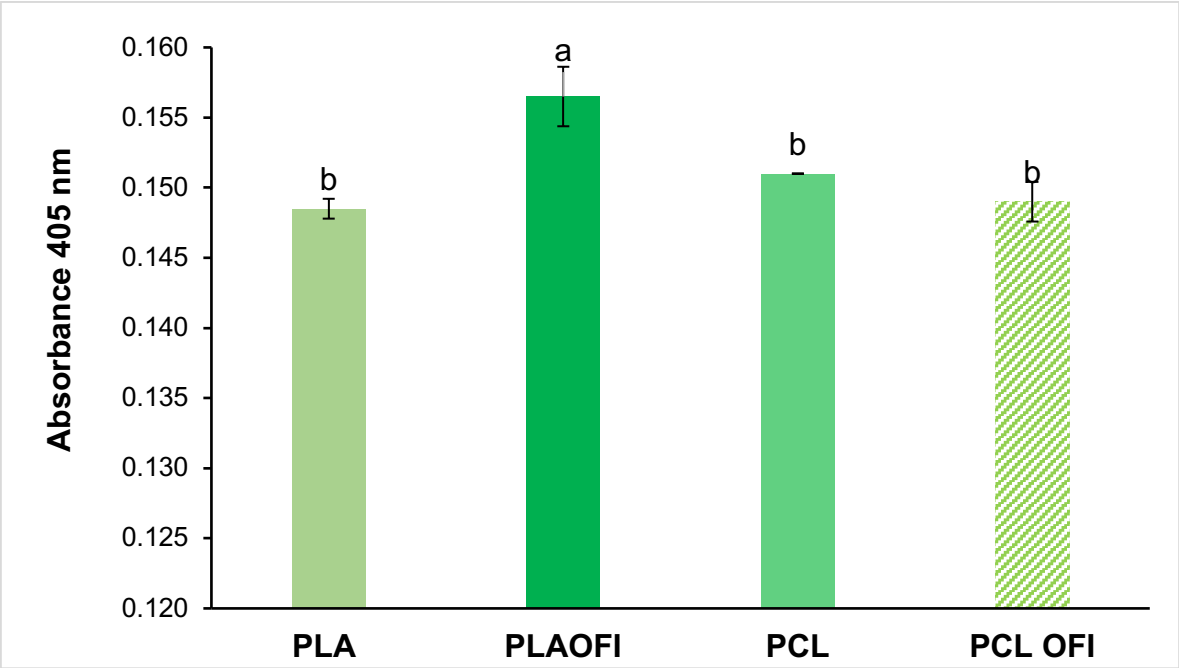


***Figure 28.*** *hFOB cell maturation (Abs) via Alkaline Phosphatase Activity (ALP) assay in polylactic acid (PLA) and polycaprolactone (PCL) electrospun nanofibers with and without Opuntia ficus-indica (OFI) flour.* $^{a,b}$*Means with different letter are significantly different p<0.05 by Tukey's test.*

## 3.12 Calcium Deposition

Calcein Green is a cell-non-permanent fluorescent dye that bounds to calcium crystals. The pattern of calcium hydroxyapatite deposition was observed in PLA and PCL nanofibers with and without OFI flour (**Figure 29**). It can be observed that PLA nanofibers had a good calcium deposition both with, and without OFI flour. On the other hand, the PCL nanofibers showed better calcium deposition with OFI flour than without it. Specifically, in PLA nanofiber, calcium deposition was homogenous, in comparison to in PLA OFI nanofiber, where it was focalized and concentrated in between cells.

On the other hand, in PCL nanofiber calcium deposition wasn't homogenous, according to the zone, it can be observed some calcium agglomeration. However, PCL OFI showed homogeneous deposition, focalized and concentrated in between cells, like in PLA OFI nanofibers. These results can be related to previous work, where it has been reported that nopal pads can be an important source of calcium (Contreras-Padilla et al., 2011).

According to the results of alkaline phosphatase (ALP) activity shown in section 3.11, it can be considered that higher ALP activity represents more mature hFOB cells, and therefore, more mineralization and calcium deposition. These results are in accordance with the previously mentioned (3.11) since in PLA fiber there is more focalized calcium deposition, which is evidence of mineralization which could be precursor to dense and thicker bone, confirming the nanofiber's potential application as a scaffold.

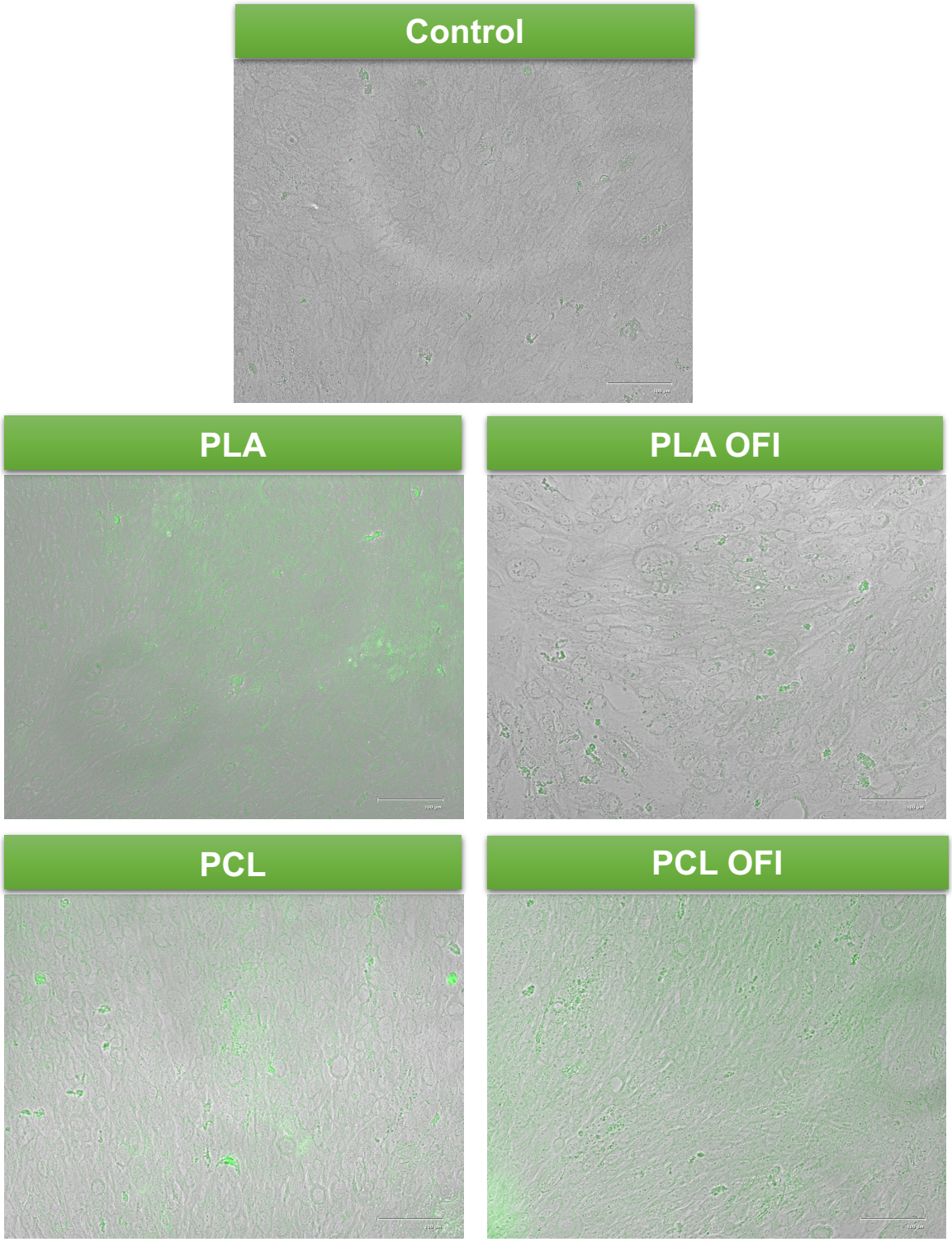


***Figure 29.*** *Calcium deposition of hFOB cells in polylactic acid (PLA) and polycaprolactone (PCL) electrospun nanofibers with and without Opuntia ficus-indica (OFI) flour.*

# 4. Conclusions and Future Perspectives

The development of PLA and PCL electrospun nanofibers with good qualitative characteristics such as a uniform mesh, easy to recover was possible. The addition of different levels of *Opuntia ficus-indica* flour was achieved which gave different characteristics to the electrospun nanofibers.

The final electrospinning parameters were 10% w/v for polymer solution with the addition of 70% w/w of OFI flour, electrospun at a distance of 15 cm, with 20 kV at a flow rate of 1mL/h. Specifically, PLA nanofibers showed a smoother appearance in comparison to the PCL nanofibers, which had a porous appearance in its surface; also, PCL nanofibers appeared to be thicker than PLA nanofibers. These characteristics , among others, are given thanks to the versatility of the electrospinning process such as solvent, polymer concentration, solvent ratio, flow rate and distance between syringe and collector.

Furthermore, by the addition of OFI flour to the nanofibers it was identified the main isorhamnetin glycosides (IG1-IG5) in the nanofibers, particularly by the addition of 10%, 30% and 50% w/w, the isorhamnetin glycosides concentration was higher in the PLA fibers by 53.51%, 63.74%, 74.92%, respectively, in comparison with the PCL fibers, but with the addition of 70% w/w of OFI flour, the PCL nanofiber allowed to load 28.46% more of isorhamnetin glycosides in comparison to the PLA nanofiber. Given this, the nanofibers with 70% of OFI flour of both polymers were selected to continue with the next assays.

The molecular interaction between the PLA and PCL polymers with the isorhamnetin glycosides was confirmed by FTIR. It was observed that when adding OFI flour to both electrospun nanofibers, OFI flour peaks disappear, and the polymer peaks lower its intensity, which is related to the involvement of the corresponding functional groups in some reactions.

The main bonds created between PLA and IGs were hydrogen bonding due to the OH provided by PLA, so it could be considered that due to the availability of several OH and C=O groups in the PLA structure, it is easier to bond with the isorhamnetin glycosides, which is why PLA nanofibers loaded with 10%, 30% and

50% w/w of OFI flour showed a higher concentration range in the PLA nanofibers loaded with 10%, 30% and 50% w/w of OFI flour, in comparison to the PCL nanofibers.

In a similar way, the main bonds created between PCL and IGs were hydrogen bonding and C-O bonding due to terminal C=O and OH groups provided by PCL. In the specific case were the IGs concentration in the PCL fibers loaded with 70% w/w of OFI flour was higher by 28.46% could be explain by a more compact stacking reached by Van der Waals interaction, which could allow better interaction between PCL and the IGs.

On the other hand, SEM morphological characterization of both PLA and PCL nanofibers loaded with 70% w/w OFI flour, showed that all fibers are randomly oriented. Specifically, PLA nanofibers presented a porous surface, with a few beads, and better alignment than PCL nanofibers, which presented a bead-like structure, which is explained by the use of high voltages. Moreover, by the addition of OFI flour to the PLA fibers it was observed a decrease of beads, and in the PCL was observed an apparent increment in the thickness of the fibers.

Concerning the release, it was observed higher isorhamnetin glycosides release percentage in the PLA nanofibers rather in the PCL nanofibers after 48h. Specifically, the IG that was easier to release in both fibers was IG3, which had higher release percentage in PLA nanofiber in comparison to the PCL nanofiber. These results could be attributed to the structure of the IG3, specifically to the nature of the sugar moiety or to the fact that IG3 is one of the most abundant glycosides found in OFI flour.

The highest biodegradation rate was observed in the PLA and PCL control fibers after 48h. In addition, the nanofibers loaded with isorhamnetin glycosides were the ones with the lower biodegradation rate, where it was observed a higher degradation rate after 24h rather than in 48h. Furthermore, the fibers loaded with isorhamnetin glycosides showed the highest swelling ratio, where PLA OFI had 89.99% and PCL OFI had 81.38%.

IGs cytotoxicity in hFOB cells was assess. There wasn’t a significant effect in the cell viability in the PLA fibers during 24h or 48h, so it can be considered that

there isn't a significant added effect on cell viability due to the isorhamnetin glycosides. On the other hand, in 24h there was a positive effect from the IGs in the hFOB cell viability in PCL fibers, however at 48h a cytotoxic effect starts showing.

Cell differentiation was observed after 7 days, where all cells showed maturation. Particularly, it can be observed that the fibers with OFI flour less visible cells in comparison to the fibers without OFI flour.

Regarding ALP activity, a positive effect of the IGs in the PLA nanofiber was observed, however, on the PCL OFI nanofibers there is no significant effect from the IGs. With this, we could assume that there is evidence of maturation and potential mineralization by the IGs in PLA nanofibers, which could enhance bone formation.

Finally, it was shown that PLA nanofibers had a good calcium deposition both with, and without OFI flour. On the other hand, the PCL nanofibers showed better calcium deposition with OFI flour than without it.

After further analysis, we can conclude that PLA electrospun nanofiber mesh loaded with 70% w/w of OFI flour presented better characteristics to be considered as scaffold for adhesion and maturation of human osteoblasts hFOB and its impact in bone regeneration *in vitro*.

Further work should consider the improvement of the solution and electrospinning parameters to obtain a better assembly, with less beads or a better alignment to favor biological activity, and therefore, to match the functionality for commercial requirements. On the other hand, it is also recommended to carry inflammation assays to detect early stages of bone formation and to get a better approach on the cellular growth and proliferation of hFOB.

# 5. Bibliography


Aceituno-Medina, M., Mendoza, S., Rodríguez, B. A., Lagaron, J. M., & López-Rubio, A. (2015). Improved antioxidant capacity of quercetin and ferulic acid during in-vitro digestion through encapsulation within food-grade electrospun fibers. *Journal of Functional Foods*, *12*, 332-341. https://doi.org/10.1016/j.jff.2014.11.028

Antunes-Ricardo, M., García-Cayuela, T., Mendiola, J. A., Ibañez, E., Gutiérrez-Uribe, J. A., Cano, M. P., & Guajardo-Flores, D. (2018). Supercritical CO2 enzyme hydrolysis as a pretreatment for the release of isorhamnetin conjugates from Opuntia ficus-indica (L.) Mill. *The Journal of Supercritical Fluids*, *141*, 21-28. https://doi.org/10.1016/j.supflu.2017.11.030

Antunes-Ricardo, M., Gutiérrez-Uribe, J. A., & Guajardo-Flores, D. (2017). Extraction of isorhamnetin conjugates from Opuntia ficus-indica (L.) Mill using supercritical fluids. *The Journal of Supercritical Fluids*, *119*, 58-63. https://doi.org/10.1016/j.supflu.2016.09.003

Antunes-Ricardo, M., Gutiérrez-Uribe, J. A., López-Pacheco, F., Alvarez, M. M., & Serna-Saldívar, S. O. (2015). In vivo anti-inflammatory effects of isorhamnetin glycosides isolated from Opuntia ficus-indica (L.) Mill cladodes. *Industrial Crops and Products*, *76*, 803-808. https://doi.org/10.1016/j.indcrop.2015.05.089

Antunes-Ricardo, M., Gutiérrez-Uribe, J. A., Martínez-Vitela, C., & Serna-Saldívar, S. O. (2015). Topical Anti-Inflammatory Effects of Isorhamnetin Glycosides Isolated from *Opuntia ficus-indica*. *BioMed Research International*, *2015*, 1-9. https://doi.org/10.1155/2015/847320

Antunes-Ricardo, M., Moreno-García, B. E., Gutiérrez-Uribe, J. A., Aráiz-Hernández, D., Alvarez, M. M., & Serna-Saldivar, S. O. (2014a). Induction of Apoptosis in Colon Cancer Cells Treated with Isorhamnetin Glycosides from Opuntia Ficus-indica Pads. *Plant Foods for Human Nutrition*, *69*(4), 331-336. https://doi.org/10.1007/s11130-014-0438-5

Antunes-Ricardo, M., Moreno-García, B. E., Gutiérrez-Uribe, J. A., Aráiz-Hernández, D., Alvarez, M. M., & Serna-Saldivar, S. O. (2014b). Induction of

Apoptosis in Colon Cancer Cells Treated with Isorhamnetin Glycosides from Opuntia Ficus-indica Pads. *Plant Foods for Human Nutrition*, *69*(4), 331-336. https://doi.org/10.1007/s11130-014-0438-5

Atallah, R., Leijendekkers, R. A., Hoogeboom, T. J., & Fr, J. P. (2018). *Complications of bone-anchored prostheses for individuals with an extremity amputation: A systematic review*. *13*(8), 23. https://doi.org/10.1371/ journal.pone.0201821

Austermann, K., Baecker, N., Stehle, P., & Heer, M. (2019). Putative Effects of Nutritive Polyphenols on Bone Metabolism In Vivo—Evidence from Human Studies. *Nutrients*, *11*(4), 871. https://doi.org/10.3390/nu11040871

Bavatharani, C., Muthusankar, E., Wabaidur, S. M., Alothman, Z. A., Alsheetan, K. M., AL-Anazy, M. mana, & Ragupathy, D. (2021). Electrospinning technique for production of polyaniline nanocomposites/nanofibres for multi-functional applications: A review. *Synthetic Metals*, *271*, 116609. https://doi.org/10.1016/j.synthmet.2020.116609

Beam, E., & Osmon, D. (2018). *Prosthetic Joint Infection Update*. 17. https://doi.org/10.1016/j.idc.2018.06.005

Behere, I., Pardawala, Z., Vaidya, A., Kale, V., & Ingavle, G. (2020). Osteogenic differentiation of an osteoblast precursor cell line using composite PCL-gelatin-nHAp electrospun nanofiber mesh. *International Journal of Polymeric Materials and Polymeric Biomaterials*, 1-15. https://doi.org/10.1080/00914037.2020.1767619

Biglia, A., Morandi, V., Monti, S., Delvino, P., Cavagna, L., & Montecucco, C. (2020). Cobalt hip prosthesis intoxication mimicking an autoimmune disease. *Joint Bone Spine*, S1297319X2030110X. https://doi.org/10.1016/j.jbspin.2020.05.014

Bijukumar, D. R., Segu, A., Souza, J. C. M., Li, X., Barba, M., Mercuri, L. G., J. Jacobs, J., & Mathew, M. T. (2018). Systemic and local toxicity of metal debris released from hip prostheses: A review of experimental approaches. *Nanomedicine: Nanotechnology, Biology and Medicine*, *14*(3), 951-963. https://doi.org/10.1016/j.nano.2018.01.001

Catanzano, O., Gomez d'Ayala, G., D'Agostino, A., Di Lorenzo, F., Schiraldi, C.,

Malinconico, M., Lanzetta, R., Bonina, F., & Laurienzo, P. (2021). PEG-crosslinked-chitosan hydrogel films for in situ delivery of Opuntia ficus-indica extract. *Carbohydrate Polymers*, *264*, 117987. https://doi.org/10.1016/j.carbpol.2021.117987

Choi, K., Choi, M.-C., Han, D.-H., Park, T.-S., & Ha, C.-S. (2013). Plasticization of poly(lactic acid) (PLA) through chemical grafting of poly(ethylene glycol) (PEG) via in situ reactive blending. *European Polymer Journal*, *49*(8), 2356-2364. https://doi.org/10.1016/j.eurpolymj.2013.05.027

Colic, K., & Sedmak, A. (2016). The current approach to research and design of the artificial hip prosthesis: A review. *Rheumatology and Orthopedic Medicine*, *1*(1). https://doi.org/10.15761/ROM.1000106

Contreras-Padilla, M., Pérez-Torrero, E., Hernández-Urbiola, M. I., Hernández-Quevedo, G., del Real, A., Rivera-Muñoz, E. M., & Rodríguez-García, M. E. (2011). Evaluation of oxalates and calcium in nopal pads (Opuntia ficus-indica var. Redonda) at different maturity stages. *Journal of Food Composition and Analysis*, *24*(1), 38-43. https://doi.org/10.1016/j.jfca.2010.03.028

Eren, E. D., Tansik, G., Tekinay, A. B., & Guler, M. O. (2018). Mineralized Peptide Nanofiber Gels for Enhanced Osteogenic Differentiation. *ChemNanoMat*, *4*(8), 837-845. https://doi.org/10.1002/cnma.201700354

Fang, R., Zhang, E., Xu, L., & Wei, S. (2010). Electrospun PCL/PLA/HA Based Nanofibers as Scaffold for Osteoblast-Like Cells. *Journal of Nanoscience and Nanotechnology*, *10*(11), 7747-7751. https://doi.org/10.1166/jnn.2010.2831

Ferreira, M. E., Pereira, M. de L., Costa, F. G. e, Sousa, J. P., & Simões de Carvalho, G. (2003). Comparative study of metallic biomaterials toxicity: A histochemical and immunohistochemical demonstration in mouse spleen. *Journal of Trace Elements in Medicine and Biology*, *17*(1), 45-49. https://doi.org/10.1016/S0946-672X(03)80045-7

García, N. L., Lamanna, M., D'Accorso, N., Dufresne, A., Aranguren, M., & Goyanes, S. (2012). Biodegradable materials from grafting of modified PLA onto starch nanocrystals. *Polymer Degradation and Stability*, *97*(10), 2021-2026. https://doi.org/10.1016/j.polymdegradstab.2012.03.032

Gheribi, R., Puchot, L., Verge, P., Jaoued-Grayaa, N., Mezni, M., Habibi, Y., & Khwaldia, K. (2018). Development of plasticized edible films from Opuntia ficus-indica mucilage: A comparative study of various polyol plasticizers. *Carbohydrate Polymers*, *190*, 204-211. https://doi.org/10.1016/j.carbpol.2018.02.085

Gibon, E., Lu, L., & Goodman, S. B. (2016). Aging, inflammation, stem cells, and bone healing. *Stem Cell Research & Therapy*, *7*(1), 44. https://doi.org/10.1186/s13287-016-0300-9

Golub, E. E., & Boesze-Battaglia, K. (2007). The role of alkaline phosphatase in mineralization. *Current Opinion in Orthopaedics*, *18*(5), 444-448. https://doi.org/10.1097/BCO.0b013e3282630851

Gong, G., Guan, Y.-Y., Zhang, Z.-L., Rahman, K., Wang, S.-J., Zhou, S., Luan, X., & Zhang, H. (2020). Isorhamnetin: A review of pharmacological effects. *Biomedicine & Pharmacotherapy*, *128*, 110301. https://doi.org/10.1016/j.biopha.2020.110301

Gundtoft, P. H. (2017). Increased Mortality After Prosthetic Joint Infection in Primary THA. *Clinical Orthopaedics and Related Research*, *475*(11), 9.

Guo, Z., Xu, J., Ding, S., Li, H., Zhou, C., & Li, L. (2015). *In vitro* evaluation of random and aligned polycaprolactone/gelatin fibers via electrospinning for bone tissue engineering. *Journal of Biomaterials Science, Polymer Edition*, *26*(15), 989-1001. https://doi.org/10.1080/09205063.2015.1065598

Habauzit, V., & Horcajada, M.-N. (2008). Phenolic phytochemicals and bone. *Phytochemistry Reviews*, *7*(2), 313-344. https://doi.org/10.1007/s11101-007-9078-9

Harborne, J. B. (1965). Plant polyphenols—XIV. *Phytochemistry*, *4*(1), 107-120. https://doi.org/10.1016/S0031-9422(00)86152-X

Hassanajili, S., Karami-Pour, A., Oryan, A., & Talaei-Khozani, T. (2019). Preparation and characterization of PLA/PCL/HA composite scaffolds using indirect 3D printing for bone tissue engineering. *Materials Science and Engineering: C*, *104*, 109960. https://doi.org/10.1016/j.msec.2019.109960

Havlíček, K., Svobodová, L., Bakalova, T., & Lederer, T. (2020). Influence of

electrospinning methods on characteristics of polyvinyl butyral and polyurethane nanofibres essential for biological applications. *Materials & Design*, *194*, 108898. https://doi.org/10.1016/j.matdes.2020.108898

Heidari, M., Bahrami, S. H., Ranjbar-Mohammadi, M., & Milan, P. B. (2019). Smart electrospun nanofibers containing PCL/gelatin/graphene oxide for application in nerve tissue engineering. *Materials Science and Engineering: C*, *103*, 109768. https://doi.org/10.1016/j.msec.2019.109768

Hernandez, C. J., Majeska, R. J., & Schaffler, M. B. (2004). Osteocyte density in woven bone. *Bone*, *35*(5), 1095-1099. https://doi.org/10.1016/j.bone.2004.07.002

Hernández-Gil, I. F.-T., Gracia, M. A. A., & Jerez, B. (2006). Physiological bases of bone regeneration I. Histology and physiology of bone tissue. *Oral Surgery*, *11*, E47-51.

Herrero-Herrero, M., Gómez-Tejedor, J. A., & Vallés-Lluch, A. (2018). PLA/PCL electrospun membranes of tailored fibres diameter as drug delivery systems. *European Polymer Journal*, *99*, 445-455. https://doi.org/10.1016/j.eurpolymj.2017.12.045

Ho, J. H., Leikin, J. B., Dargan, P. I., Archer, J. R. H., Wood, D. M., & Brent, J. (2017). Metal-on-Metal Hip Joint Prostheses: A Retrospective Case Series Investigating the Association of Systemic Toxicity with Serum Cobalt and Chromium Concentrations. *Journal of Medical Toxicology*, *13*(4), 321-328. https://doi.org/10.1007/s13181-017-0629-1

Hokmabad, V. R., Davaran, S., Aghazadeh, M., Alizadeh, E., Salehi, R., & Ramazani, A. (2019). Effect of incorporating Elaeagnus angustifolia extract in PCL-PEG-PCL nanofibers for bone tissue engineering. *Frontiers of Chemical Science and Engineering*, *13*(1), 108-119. https://doi.org/10.1007/s11705-018-1742-7

Hosseini-Koupaei, M., Shareghi, B., Saboury, A. A., Davar, F., & Raisi, F. (2016). The effect of spermidine on the structure, kinetics and stability of proteinase K: Spectroscopic and computational approaches. *RSC Advances*, *6*(107), 105476-105486. https://doi.org/10.1039/C6RA20975K

Huang, R.-L., Yuan, Y., Tu, J., Zou, G.-M., & Li, Q. (2014). Opposing TNF-α/IL-1β- and BMP-2-activated MAPK signaling pathways converge on Runx2 to regulate BMP-2-induced osteoblastic differentiation. *Cell Death & Disease*, *5*(4), e1187-e1187. https://doi.org/10.1038/cddis.2014.101

INEGI. (2019). *Estadísticas a propósito del Día Internacional de las Personas de Edad (1º de octubre) Datos Nacionales* (Comunicado de Prensa N.º 475/19; pp. 1-9). INEGI; edad2019_Nal.

Jelsma, J., Kleinveld, H., Rozemuller, A., & Heyligers, I. (2020). *Neurology in metal-on-metal hip arthroplasty a case of suspected prosthetic hip-associated cobalt toxicity*. *86 e-supplement*(1), 67-70.

Ji-Heui, K., Chan-Hum, P., Ok-Joo, L., Jung-Min, L., Jong-Wook, K., Young-Hwan, P., & Chang-Seok, K. (2012). Preparation and in vivo degradation of controlled biodegradability of electrospun silk fibroin nanofiber mats. *Journal of Biomedical Materials Research A*, *00A*(00), 1-9. https://doi.org/10.1002/jbm.a.34274

Jiménez-Rodríguez, A., Heredia-Olea, E., Barba-Dávila, B. A., Gutiérrez-Uribe, J. A., & Antunes-Ricardo, M. (2021). Polysaccharides from Agave salmiana bagasse improves the storage stability and the cellular uptake of indomethacin nanoemulsions. *Food and Bioproducts Processing*, *127*, 114-127. https://doi.org/10.1016/j.fbp.2021.02.008

Jin, J. Y., Choi, E. Y., Park, H. R., Choi, J. I., Choi, I. S., & Kim, S. J. (2013). Isorhamnetin inhibits Prevotella intermedia lipopolysaccharide-induced production of interleukin-6 in murine macrophages via anti-inflammatory heme oxygenase-1 induction and inhibition of nuclear factor- kB and signal transducer and activator of transcription 1 activation. *Journal of Periodontal Research*, *48*(6), 687-695. https://doi.org/10.1111/jre.12054

Jindal, A., Mondal, T., & Bhattacharya, J. (2020). An in vitro evaluation of zinc silicate fortified chitosan scaffolds for bone tissue engineering. *International Journal of Biological Macromolecules*, *164*, 4252-4262. https://doi.org/10.1016/j.ijbiomac.2020.09.018

Karadeniz, F., Kim, J.-A., Ahn, B.-N., Kwon, M., & Kong, C.-S. (2014). Effect of

Salicornia herbacea on Osteoblastogenesis and Adipogenesis in Vitro. *Marine Drugs*, *12*(10), 5132-5147. https://doi.org/10.3390/md12105132

Khoshnoudi-Nia, S., Sharif, N., & Jafari, S. M. (2020). Loading of phenolic compounds into electrospun nanofibers and electrosprayed nanoparticles. *Trends in Food Science & Technology*, *95*, 59-74. https://doi.org/10.1016/j.tifs.2019.11.013

Ko, J. H., Yin, H., An, J., & Chung, D. J. (2010). Characterization of Cross-linked Gelatin Nanofibers through Electrospinning. *Macromolecular Research*, *18*(2), 137-143. https://doi.org/10.1007/s13233-009-0103-2

Komori, T. (2006). Regulation of osteoblast differentiation by transcription factors. *Journal of Cellular Biochemistry*, *99*(5), 1233-1239. https://doi.org/10.1002/jcb.20958

Komori, T. (2009). Regulation of Osteoblast Differentiation by Runx2. En Y. Choi (Ed.), *Osteoimmunology* (Vol. 658, pp. 43-49). Springer US. https://doi.org/10.1007/978-1-4419-1050-9_5

Lacey, D. C., Simmons, P. J., Graves, S. E., & Hamilton, J. A. (2009). Proinflammatory cytokines inhibit osteogenic differentiation from stem cells: Implications for bone repair during inflammation. *Osteoarthritis and Cartilage*, *17*(6), 735-742. https://doi.org/10.1016/j.joca.2008.11.011

Lenguerrand, E., Whitehouse, M. R., Beswick, A. D., Jones, S. A., Porter, M. L., & Blom, A. W. (2017). *Revision for prosthetic joint infection following hip arthroplasty*. *6*(6), 8.

Liu, Y., Lim, J., & Teoh, S.-H. (2013). Review: Development of clinically relevant scaffolds for vascularised bone tissue engineering. *Biotechnology Advances*, *31*(5), 688-705. https://doi.org/10.1016/j.biotechadv.2012.10.003

Lu, M., & Zhao, X.-H. (2018). The Growth Proliferation, Apoptotic Prevention, and Differentiation Induction of the Gelatin Hydrolysates from Three Sources to Human Fetal Osteoblasts (hFOB 1.19 Cells). *Molecules*, *23*(6), 1287. https://doi.org/10.3390/molecules23061287

Maruyama, M., Rhee, C., Utsunomiya, T., Zhang, N., Ueno, M., Yao, Z., & Goodman, S. B. (2020). Modulation of the Inflammatory Response and Bone Healing.

*Frontiers in Endocrinology*, *11*, 386. https://doi.org/10.3389/fendo.2020.00386

Mehteroğlu, E., Çakmen, A. B., Aksoy, B., Balcıoğlu, S., Köytepe, S., Ateş, B., & Yılmaz, İ. (2020). Preparation of hybrid PU/PCL fibers from steviol glycosides via electrospinning as a potential wound dressing materials. *Journal of Applied Polymer Science*, *137*(40), 49217. https://doi.org/10.1002/app.49217

Mohandesnezhad, S., Pilehvar-Soltanahmadi, Y., Alizadeh, E., Goodarzi, A., Davaran, S., Khatamian, M., Zarghami, N., Samiei, M., Aghazadeh, M., & Akbarzadeh, A. (2020). In vitro evaluation of Zeolite-nHA blended PCL/PLA nanofibers for dental tissue engineering. *Materials Chemistry and Physics*, *252*, 123152. https://doi.org/10.1016/j.matchemphys.2020.123152

Moniz, S., Hodgkinson, S., & Yates, P. (2017). Cardiac transplant due to metal toxicity associated with hip arthroplasty. *Arthroplasty Today*, *3*(3), 151-153. https://doi.org/10.1016/j.artd.2017.01.005

Morris, A. H., Stamer, D. K., & Kyriakides, T. R. (2017). The host response to naturally-derived extracellular matrix biomaterials. *Seminars in Immunology*, *29*, 72-91. https://doi.org/10.1016/j.smim.2017.01.002

Murr, L. E. (2017). Open-cellular metal implant design and fabrication for biomechanical compatibility with bone using electron beam melting. *Journal of the Mechanical Behavior of Biomedical Materials*, *76*, 164-177. https://doi.org/10.1016/j.jmbbm.2017.02.019

Otálora, M. C., Gómez Castaño, J. A., & Wilches-Torres, A. (2019). Preparation, study and characterization of complex coacervates formed between gelatin and cactus mucilage extracted from cladodes of Opuntia ficus-indica. *LWT*, *112*, 108234. https://doi.org/10.1016/j.lwt.2019.06.001

Paragkumar N, T., Edith, D., & Six, J.-L. (2006). Surface characteristics of PLA and PLGA films. *Applied Surface Science*, *253*(5), 2758-2764. https://doi.org/10.1016/j.apsusc.2006.05.047

Peng, S., & Ilango, P. R. (2020). *Electrospinning of Nanofibers for Battery Applications*. Springer Singapore. https://doi.org/10.1007/978-981-15-1428-9

Preez, I. du, Richter, W., Papendorp, D. van, & Joubert, A. (2018). hFOB 1.19

osteoblast cells grown on a biomimetic biphasic nanoscaffold: An in vitro evaluation for possible bone tissue engineering. *Biomedical Research*, *29*(11). https://doi.org/10.4066/biomedicalresearch.67-17-2720

Prentice, A. (2004). Diet, nutrition and the prevention of osteoporosis. *Public Health Nutrition*, *7*(1a), 227-243. https://doi.org/10.1079/PHN2003590

Rabiatul, A. R., Lokanathan, Y., Rohaina, C. M., Chowdhury, S. R., Aminuddin, B. S., & Ruszymah, B. H. I. (2015). Surface modification of electrospun poly(methyl methacrylate) (PMMA) nanofibers for the development of *in vitro* respiratory epithelium model. *Journal of Biomaterials Science, Polymer Edition*, *26*(17), 1297-1311. https://doi.org/10.1080/09205063.2015.1088183

Rahmy, A. I. A., Gosens, T., Blake, G. M., Tonino, A., & Fogelman, I. (2004). Periprosthetic bone remodelling of two types of uncemented femoral implant with proximal hydroxyapatite coating: A 3-year follow-up study addressing the influence of prosthesis design and preoperative bone density on periprosthetic bone loss. *Osteoporosis International*, *15*(4), 281-289. https://doi.org/10.1007/s00198-003-1546-5

Ramírez-Fernández, O., Godínez, R., Morales, J., Gómez-Quiroz, L. E., Gutiérrez-Ruiz, M. C., Zúñiga-Aguilar, E., & Olayo, R. (2013). Crecimiento Volumétrico de Hepatocitos en Estructuras Basadas en Biomateriales Modificados Superficialmente. En J. Folgueras Méndez, T. Y. Aznielle Rodríguez, C. F. Calderón Marín, S. B. Llanusa Ruiz, J. Castro Medina, H. Vega Vázquez, M. Carballo Barreda, & R. Rodríguez Rojas (Eds.), *V Latin American Congress on Biomedical Engineering CLAIB 2011 May 16-21, 2011, Habana, Cuba* (Vol. 33, pp. 104-107). Springer Berlin Heidelberg. https://doi.org/10.1007/978-3-642-21198-0_27

Redlich, K., & Smolen, J. S. (2012). Inflammatory bone loss: Pathogenesis and therapeutic intervention. *Nature Reviews Drug Discovery*, *11*(3), 234-250. https://doi.org/10.1038/nrd3669

Rezaeinia, H., Emadzadeh, B., & Ghorani, B. (2020). Electrospun balangu (Lallemantia royleana) hydrocolloid nanofiber mat as a fast-dissolving carrier for bergamot essential oil. *Food Hydrocolloids*, *100*, 105312.

https://doi.org/10.1016/j.foodhyd.2019.105312

Sabokbar, A., Millett, P. J., Myer, B., & Rushton, N. (1994). A rapid, quantitative assay for measuring alkaline phosphatase activity in osteoblastic cells in vitro. *Bone and Mineral*, *27*(1), 57-67. https://doi.org/10.1016/S0169-6009(08)80187-0

Santos-Zea, L., Gutiérrez-Uribe, J. A., & Serna-Saldivar, S. O. (2011). Comparative Analyses of Total Phenols, Antioxidant Activity, and Flavonol Glycoside Profile of Cladode Flours from Different Varieties of Opuntia spp. *Journal of Agricultural and Food Chemistry*, *59*(13), 7054-7061. https://doi.org/10.1021/jf200944y

Su, X., Sun, K., Cui, F. Z., & Landis, W. J. (2003). Organization of apatite crystals in human woven bone. *Bone*, *32*(2), 150-162. https://doi.org/10.1016/S8756-3282(02)00945-6

Thomas, S. W., Alcantar, N. A., & Pais, Y. (2012). **Electrospinning and Characterization of Novel *Opuntia ficus-indica* Mucilage Biomembrane** . *MRS Proceedings*, *1480*, imrc12-1480-s2b-0017. https://doi.org/10.1557/opl.2012.1614

Uppal, R., Ramaswamy, G. N., Arnold, C., Goodband, R., & Wang, Y. (2011). Hyaluronic acid nanofiber wound dressing-production, characterization, and in vivo behavior. *Journal of Biomedical Materials Research Part B: Applied Biomaterials*, *97B*(1), 20-29. https://doi.org/10.1002/jbm.b.31776

Urbaniak-Domagala, W. (2013). Electrical properties of polylactides. *Journal of Electrostatics*, *71*(3), 456-461. https://doi.org/10.1016/j.elstat.2013.01.008

Vaz, S., Ferreira, T. C., Salgado, L., & Paycha, F. (2017). Bone scan usefulness in patients with painful hip or knee prosthesis: 10 situations that can cause pain, other than loosening and infection. *European Journal of Orthopaedic Surgery & Traumatology*, *27*(2), 147-156. https://doi.org/10.1007/s00590-016-1884-6

Wang, Y., Guo, H., & Ying, D. (2013). Multilayer scaffold of electrospun PLA-PCL-collagen nanofibers as a dural substitute: PLA-PCL-Collagen as a Dural Substitute. *Journal of Biomedical Materials Research Part B: Applied Biomaterials*, *101*(8), 1359-1366. https://doi.org/10.1002/jbm.b.32953

Xue, J., Wu, T., Dai, Y., & Xia, Y. (2019). Electrospinning and Electrospun Nanofibers: Methods, Materials, and Applications. *Chemical Reviews*, *119*(8), 5298-5415. https://doi.org/10.1021/acs.chemrev.8b00593

Yang, C., Chen, S., Wang, J., Zhu, T., Xu, G., Chen, Z., Ma, X., & Li, W. (2016). A facile electrospinning method to fabricate polylactide/graphene/MWCNTs nanofiber membrane for tissues scaffold. *Applied Surface Science*, *362*, 163-168. http://dx.doi.org/10.1016/j.apsusc.2015.11.142

Young, M. F. (2003). Bone Matrix Proteins: More Than Markers. *Calcified Tissue International*, *72*(1), 2-4. https://doi.org/10.1007/s00223-002-1017-6

Zaarour, B., Zhu, L., Huang, C., & Jin, X. (2020). A mini review on the generation of crimped ultrathin fibers via electrospinning: Materials, strategies, and applications. *Polymers for Advanced Technologies*, *31*(7), 1449-1462. https://doi.org/10.1002/pat.4876

Zadeh, K. M., Luyt, A. S., Zarif, L., Augustine, R., Hasan, A., Messori, M., Hassan, M. K., & Yalcin, H. C. (2019). Electrospun polylactic acid/date palm polyphenol extract nanofibres for tissue engineering applications. *Emergent Materials*, *2*(2), 141-151. https://doi.org/10.1007/s42247-019-00042-8

Zhang, D., Li, L., Shan, Y., Xiong, J., Hu, Z., Zhang, Y., & Gao, J. (2019). In vivo study of silk fibroin/gelatin electrospun nanofiber dressing loaded with astragaloside IV on the effect of promoting wound healing and relieving scar. *Journal of Drug Delivery Science and Technology*, *52*, 272-281. https://doi.org/10.1016/j.jddst.2019.04.021

Zhang, Y., Kang, X., Chen, L., Pan, C., Yao, Y., & Gu, Z.-Z. (2008). Fiber-packed SPE tips based on electrospun fibers. *Analytical and Bioanalytical Chemistry*, *391*(6), 2189-2197. https://doi.org/10.1007/s00216-008-2145-2

Zhao, L., He, C., Gao, Y., Cen, L., Cui, L., & Cao, Y. (2008). Preparation and cytocompatibility of PLGA scaffolds with controllable fiber morphology and diameter using electrospinning method. *Journal of Biomedical Materials Research Part B: Applied Biomaterials*, *87B*(1), 26-34. https://doi.org/10.1002/jbm.b.31060

# 6. Curriculum Vitae

Master's students Kathya Huesca Urióstegui was born in Xalapa, Veracruz, México, on November 24th, 1995. She earned the Nanotechnology and Chemical Engineering from the *Instituto Tecnológico y de Estudios Superiores de Monterrey,* Monterrey Campus in May 2019. She was accepted in the graduate program in Biotechnology in August 2019.

This document was typed in using Microsoft Word® by Kathya Huesca Urióstegui